

RESEARCH ARTICLE

Tricellulin regulates junctional tension of epithelial cells at tricellular contacts through Cdc42

Yukako Oda¹, Tetsuhisa Otani², Junichi Ikenouchi^{3,4} and Mikio Furuse^{1,5,6,*}

ABSTRACT

When the surface view of each epithelial cell is compared with a polygon, its sides correspond to cell–cell junctions, whereas its vertices correspond to tricellular contacts, whose roles in epithelial cell morphogenesis have not been well studied. Here, we show that tricellulin (also known as MARVELD2), which is localized at tricellular contacts, regulates F-actin organization through Cdc42. Tricellulin-knockdown epithelial cells exhibit irregular polygonal shapes with curved cell borders and impaired organization of F-actin fibers around tricellular contacts during cell–cell junction formation. The N-terminal cytoplasmic domain of tricellulin binds to the Cdc42 guanine-nucleotide-exchange factor (GEF) Tuba (also known as DNMBP and ARHGEF36), and activates Cdc42. A tricellulin mutant that lacks the ability to bind Tuba cannot rescue the curved cell border phenotype of tricellulin-knockdown cells. These findings indicate that tricellular contacts play crucial roles in regulating the actomyosin-mediated apical junctional complex tension through the tricellulin–Tuba–Cdc42 system.

KEY WORDS: Cell–cell junction, Tricellulin, MARVELD2, Tuba, Cdc42, F-actin, Epithelial cell

INTRODUCTION

The tensile force generated by contraction of actomyosin filaments controls a variety of biological processes by regulating cellular organization and behavior. In epithelial cells, the apical junctional complex (AJC) is thought to play crucial roles in actomyosin-related cell behavior. In vertebrates, the AJC consists of adherens junctions and tight junctions, which are closely associated with each other and circumscribe the apical part of the lateral membrane (Farquhar and Palade, 1963). The AJC is delineated by thick actin filaments, called circumferential actin bundles, which cooperate with myosin II to generate tensile force (Gumbiner, 2005; Yonemura, 2011). The signaling pathways of small G proteins, including Cdc42, Rho and their effectors, which regulate F-actin polymerization and myosin II activation, are involved in this process (Jaffe and Hall, 2005; Smutny et al., 2010; Yamada and Nelson, 2007). The

combination of strong cell–cell adhesion and the tension of the underlying actomyosin bundles at the AJC controls the shape of the epithelial cell border, the morphogenesis of epithelial cellular sheets and the remodeling of epithelial cells during development (Lecuit and Lenne, 2007; Lecuit et al., 2011; Vichas and Zallen, 2011).

When the apico-lateral border of each epithelial cell is compared with a polygon, its sides correspond to cell–cell junctions and its vertices correspond to tricellular contacts, where the corners of three epithelial cells meet. Tricellular contacts can be considered to be the points that support the tensile force of actomyosin along cell–cell junctions (Cavey and Lecuit, 2009; Yonemura, 2011). Consistently, computer simulations based on this notion reproduce the shape of polygonal epithelial cells observed in true epithelial cellular sheets (Honda, 1983; Honda and Eguchi, 1980; Honda et al., 1982). Coordinated elongation and shortening of the cell–cell junctions between tricellular contacts allows rearrangement of epithelial cells within the cellular sheet during morphogenesis, leading to the idea that tricellular contacts are regulatory units for epithelial rearrangement (Cavey and Lecuit, 2009). However, the implications for tricellular contacts in the generation of tensile force along cell–cell junctions have not been demonstrated at the molecular level.

Recently, two types of integral membrane proteins, tricellulin (also known as MARVELD2) and angulin family proteins, including angulin-1 (also known as LSR), angulin-2 (also known as ILDR1) and angulin-3 (also known as ILDR2), have been identified as molecular constituents of tricellular contacts (Higashi et al., 2013; Ikenouchi et al., 2005; Masuda et al., 2011). Both types of proteins are localized at specialized tight junction structures at tricellular contacts, named tricellular tight junctions (tTJs). Angulins recruit tricellulin to tTJs and RNA interference (RNAi)-mediated knockdown studies in cultured epithelial cells have revealed that tricellulin and angulins are involved in tTJ formation as well as the full barrier function of epithelial cellular sheets (Higashi et al., 2013; Ikenouchi et al., 2005; Masuda et al., 2011). Tricellulin is a member of the tight-junction-associated Marvel protein family, which consists of occludin, tricellulin and Marvel3, and all have four transmembrane domains (Ikenouchi et al., 2005; Raleigh et al., 2010; Steed et al., 2009). In contrast to occludin and Marvel3, tricellulin has a long N-terminal cytoplasmic region. Tricellulin associates with claudins, major intramembrane components of tight junctions, within the plasma membrane and increases the complexity of the morphology of claudin-based tight junction structures reconstituted in fibroblasts (Ikenouchi et al., 2008). Mutations in the human tricellulin gene cause a recessive nonsyndromic familial deafness (DFNB49) (Riazuddin et al., 2006) and a tricellulin gene knock-in mouse that mimics one of the human tricellulin gene mutations in DFNB49 shows hearing loss with degeneration of hair cells after birth and disorganized

¹Division of Cell Biology, Department of Physiology and Cell Biology, Kobe University Graduate School of Medicine, Kobe 650-0017, Japan. ²Laboratory for Morphogenetic Signaling, RIKEN Center for Developmental Biology, Chuo-ku, Kobe 650-0047, Japan. ³Department of Biology, Faculty of Sciences, Kyushu University, Kyushu, 812-8581, Japan. ⁴PRESTO, Japan Science and Technology Agency, Saitama 332-0012, Japan. ⁵Division of Cerebral Structure, National Institute for Physiological Sciences, Okazaki 444-8787, Japan. ⁶Department of Physiological Sciences, The Graduate School for Advanced Studies, Okazaki 444-8585, Japan.

*Author for correspondence (furuse@nips.ac.jp)

tTJ structures (Nayak et al., 2013). However, the detailed molecular mechanism of tricellulin function remains elusive.

In the present study, we show that tricellulin binds to the Cdc42 guanine-nucleotide-exchange factor (GEF) Tuba (also known as DNMBP and ARHGEF36), and activates Cdc42, thereby accelerating organization of F-actin fibers at tricellular contacts. Our findings suggest a role for tricellular contacts in regulating the shape and behavior of epithelial cells through actomyosin tension.

RESULTS

Tricellulin regulates the configuration of apical cell–cell junctions in epithelial cells

To investigate the possible involvement of tricellular contacts in the maintenance of tensile force along the AJC, we generated several epithelial cell lines in which the expression of tricellulin was suppressed by tricellulin-specific small hairpin RNAs (shRNAs). By analyzing immunofluorescence staining of the AJC, we found that tricellulin-knockdown mouse MTD-1A mammary gland epithelial cells, before reaching saturation density at 48 h after plating, exhibited altered morphology in two aspects (Fig. 1A–E). First, the outlines of the cells at the level of the AJC were distorted (Fig. 1A). Quantitative analyses of the relative junctional lengths between vertices revealed that the AJC of tricellulin-knockdown cells was indeed curved (Fig. 1C). Second, ‘rosette-like’ structures, where the vertices of many cells meet, were more apparent in tricellulin-knockdown cells compared to the parental MTD-1A cells (Fig. 1D; supplementary material Fig. S1A). TUNEL assays revealed that the rosette-like structures were not caused by cell extrusion from the cellular sheet after apoptosis (supplementary material Fig. S1B). Consistent with the rosette-like structures, the circularity index of the cells, indicating the extent to which the polygonal shape of the cells resembles a circle, in tricellulin-knockdown cells was lower than the parental cells (Fig. 1E). Overexpression of an RNA interference (RNAi)-resistant tricellulin transgene into the tricellulin-knockdown cells rescued these effects (Fig. 1A–E). When the cells had mostly reached confluence at 72 h after plating, the morphological changes of tricellulin-knockdown MTD-1A cells became less remarkable (Fig. 1A). Similar morphological changes were observed in tricellulin-knockdown Caco-2 cells, a human colorectal adenocarcinoma line, at 48 h after plating (Fig. 1F–I). These findings suggest that tricellulin is involved in the junctional configuration of epithelial cells during cell–cell junction formation.

Tricellulin is involved in F-actin organization at the region of cell vertices

During intensive investigations, we further identified F-actin fibers that came up transiently at the region of prospective cell vertices, designated premature epithelial cell corners (PECs), in subconfluent MTD-1A cells after 24 h of plating (Fig. 2A). These F-actin fibers connected one PEC to another PEC (supplementary material Fig. S2A). These PEC–PEC fibers were markedly decreased in tricellulin-knockdown cells, and restored after re-expression of HA-tagged tricellulin in these cells (tricellulin-rescue cells) (Fig. 2A). The same features in the organization of F-actin were observed in mouse EpH4 mammary gland epithelial cells after cells were switched from a low- Ca^{2+} medium into a Ca^{2+} -containing medium (Fig. 2B,C; supplementary material Fig. S2A). These findings indicate that tricellulin is involved in the generation of specialized F-actin fibers running between PECs during cell–cell junction formation.

To investigate whether the F-actin fibers formed at PECs in MTD-1A cells at 24 h after plating were under tension, we examined the di-phosphorylation of myosin II regulatory light chain, an indicator of actomyosin contraction, by immunofluorescence staining (Watanabe et al., 2007). As shown in Fig. 2D, immunolabeling of diphosphorylated myosin II regulatory light chain was clearly detected along F-actin fibers between PECs in the parental MTD-1A cells and tricellulin-rescue cells, but not in tricellulin-knockdown cells. Furthermore, a monoclonal antibody that recognizes an epitope of α -catenin that is dependent on F-actin-mediated pulling force (Yonemura et al., 2010) strongly labeled cell–cell contacts around PECs in MTD-1A and tricellulin-rescue cells, but not in tricellulin-knockdown cells (Fig. 2E). At 72 h after plating, when the cells had reached saturation density, the PEC–PEC fibers of F-actin disappeared in MTD-1A cells (Fig. 2F). Immunolabeling of the pulling-force-dependent α -catenin epitope in MTD-1A cells was much decreased and could not be distinguished from the labeling in tricellulin-knockdown cells (Fig. 2F). These results suggest that tricellulin is involved in the generation of actomyosin tension between PECs at the subconfluent stage during cell–cell junction formation.

Tricellulin recruits F-actin and myosin IIB

We further found that overexpression of tricellulin in mouse mammary gland epithelial EpH4 cells sometimes produced clusters of tricellulin aggregates on bicellular cell–cell contacts, where F-actin and myosin IIB were concentrated, suggesting that tricellulin promoted F-actin recruitment (Fig. 3A). When deletion constructs of tricellulin lacking its N-terminal or C-terminal cytoplasmic domain, named tricellulin Δ N and tricellulin Δ C, respectively (Fig. 3B), were overexpressed in EpH4 cells, F-actin was concentrated into tricellulin Δ C clusters, but not tricellulin Δ N clusters (Fig. 3C). F-actin aggregation was also not observed in the tricellulin mutant lacking amino acids 1–124 in the N-terminal cytoplasmic region of tricellulin (tricellulin Δ 124) (Fig. 3C). Conversely, the clusters of a chimeric construct in which amino acids 1–124 of tricellulin were fused to the N-terminus of connexin 26 at bicellular cell–cell contacts recruited F-actin, whereas those of native connexin 26 did not (Fig. 3C). These findings suggest that amino acids 1–124 of tricellulin induce F-actin recruitment.

Tricellulin interacts with the Cdc42 GEF Tuba

To examine the mechanism behind the tricellulin-mediated F-actin organization, we investigated the molecular interactions of the N-terminal cytoplasmic region of tricellulin. By yeast two-hybrid screening with a bait containing amino acids 1–124 of tricellulin, we identified two independent clones encoding the C-terminal fragments of the Cdc42 GEF Tuba (Fig. 4A) (Otani et al., 2006; Salazar et al., 2003). Tuba contains four SH3 domains, one DH domain, one BAR domain and two SH3 domains, in that order from the N-terminus (Fig. 4A). The DH domain is responsible for the GEF activity for Cdc42, which regulates F-actin formation. Both Tuba fragments obtained in the screening contained the sixth SH3 domain at the C-terminus. An immunoprecipitation assay revealed that exogenously expressed full-length tricellulin and tricellulin Δ C interacted with endogenous Tuba in HEK293 cells, whereas tricellulin Δ N did not (Fig. 4B,C). Taken together, these findings indicate that the N-terminal cytoplasmic region of tricellulin interacts with the C-terminal SH3 domain of Tuba.

The N-terminal cytoplasmic region of tricellulin contains a proline-rich domain between amino acids 46–57 (PLPPPPLPLQPP) in mice

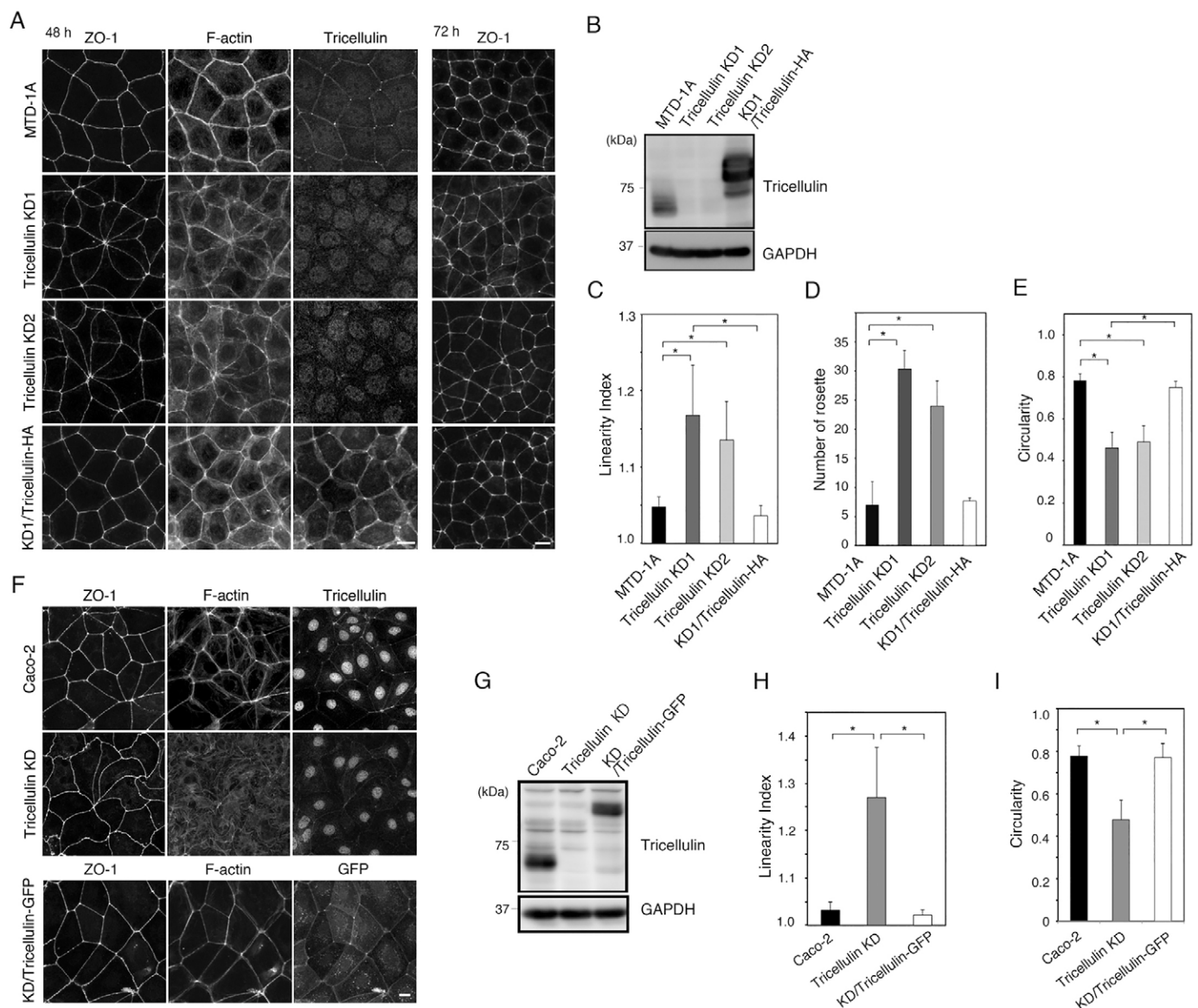


Fig. 1. Tricellulin regulates junctional configuration and actomyosin organization in epithelial cells during cell-cell junction formation. (A) Triple immunofluorescence staining of parental MTD-1A cells, two stable clones of tricellulin-knockdown MTD-1A cells (Tricellulin KD1 and Tricellulin KD2) and a stable clone of Tricellulin KD1 cells expressing shRNA-resistant tricellulin with three HA tags (KD1/Tricellulin-HA) at 48 h after plating with fluorescently labeled phalloidin and antibodies against ZO-1 and tricellulin (left). The right panel shows immunofluorescence staining of these cells at 72 h with anti-ZO-1 antibody. (B) Immunoblotting of a series of the MTD-1A cells shown in A with antibodies against tricellulin and GAPDH. (C) Quantification of junction linearity in a series of MTD-1A cells at 48 h after plating shown in A. * $P < 0.0001$. (D) Quantification of rosette-like structures in a series of MTD-1A cells at 48 h after plating shown in A. * $P < 0.01$. (E) Quantification of circularity in a series of MTD-1A cells at 48 h after plating shown in A. * $P < 0.0001$. (F) Immunofluorescence staining of Caco-2 cells, tricellulin-siRNA-treated Caco-2 cells (Tricellulin KD) and a tricellulin siRNA-treated Caco-2 clone stably expressing GFP-tagged mouse tricellulin (KD/Tricellulin-GFP) at 48 h after plating using fluorescently labeled phalloidin and an anti-ZO-1 antibody. GFP was detected by its native fluorescence. (G) Immunoblotting of a series of Caco-2 cells shown in F using antibodies against tricellulin and GAPDH. (H) Quantification of junction linearity of a series of Caco-2 cells shown in F. * $P < 0.0001$. (I) Quantification of circularity in a series of Caco-2 cells shown in F. * $P < 0.0001$. Scale bars: 10 μ m.

(Fig. 4D), and this feature of the amino acid sequence is conserved among vertebrate species (data not shown). Given that many SH3 domains are known to interact with proline-rich domains of proteins containing the minimum motif of PxxP (Feller et al., 1994), we examined the binding between the proline cluster of the N-terminal cytoplasmic region of tricellulin and Tuba. When an HA-tagged tricellulin mutant in which all of the proline residues within amino acids 48–53 were replaced with alanine residues (tricellulin-P48-53A) was expressed in HEK293 cells, interaction of endogenous Tuba with tricellulin-P48-53A was not detected in

immunoprecipitation assays with anti-HA antibody (Fig. 4D,E). *In vitro* pull-down assays also showed that a bacterial fusion protein of amino acids 1291–1580 of mouse Tuba containing the fifth and sixth SH3 domains with maltose-binding protein bound to a fusion protein of amino acids 1–150 of tricellulin with GST, but not to its mutant in which the proline residues within amino acids 48–53 were replaced with alanine residues (Fig. 4F). These results suggest that the proline-rich domain in the N-terminal cytoplasmic region of tricellulin directly binds to the C-terminal SH3 domain of Tuba.

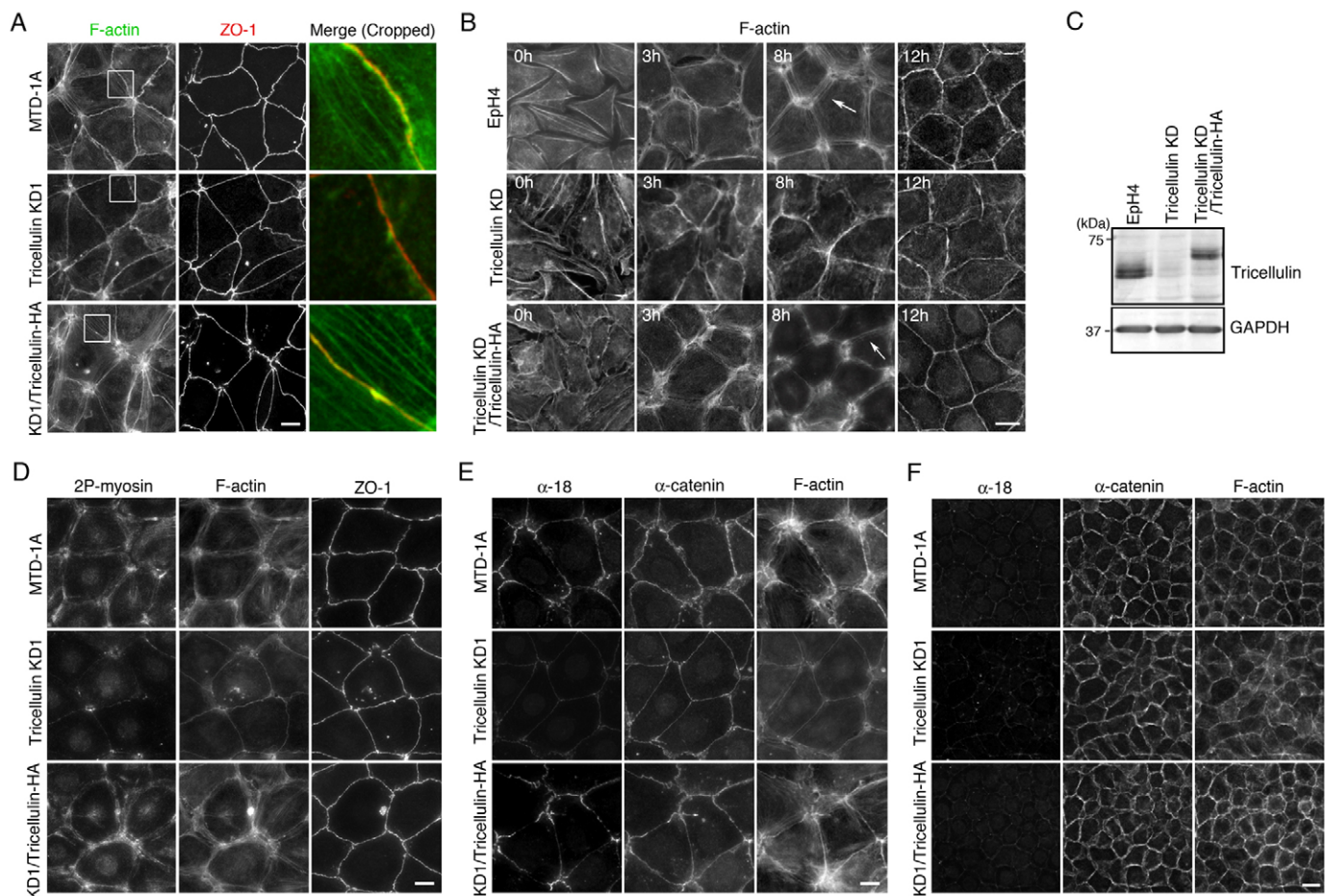


Fig. 2. Role of tricellulin in actin fiber formation during cell–cell junction assembly in epithelial cells. (A) Immunofluorescence staining of MTD-1A cells, a stable clone of tricellulin-knockdown MTD-1A cells (Tricellulin KD1) cells and tricellulin-rescue cells (KD1/Tricellulin-HA) cells in a subconfluent condition at 24 h after plating with an anti-ZO-1 antibody and fluorescently labeled phalloidin. F-actin fibers that bridge the vertices of cells are present in MTD-1A cells and KD1/Tricellulin-HA cells. These F-actin fibers are not clear in Tricellulin KD1 cells. An enlarged view of the boxed area is shown in the 'Merge' panels. (B) Eph4 cells, tricellulin-knockdown Eph4 cells (Tricellulin KD) and Tricellulin KD cells expressing HA-tagged shRNA-resistant tricellulin (Tricellulin KD/tricellulin-HA) cultured in low- Ca^{2+} medium and the same cells at 3, 8 and 12 h after a switch into a Ca^{2+} -containing medium were labeled with fluorescently labeled phalloidin to visualize F-actin. Geometric patterns of F-actin fibers between cell vertices are observed in Eph4 cells and Tricellulin KD/tricellulin-HA cells, but not in Tricellulin KD cells. (C) Western blotting analyses of Eph4, Tricellulin KD and Tricellulin KD/tricellulin-HA cells with anti-tricellulin and anti-GAPDH antibodies. (D) Immunofluorescence staining of MTD-1A, Tricellulin KD1 and KD1/tricellulin-HA cells after culture for 24 h with fluorescently labeled phalloidin (F-actin) and antibodies against di-phosphorylated myosin (2P-myosin) and ZO-1. (E,F) Triple immunofluorescence staining of MTD-1A cells at 24 h (E) and at 72 h (F) after plating with the α -18 anti- α -catenin rat monoclonal antibody, an anti- α -catenin rabbit polyclonal antibody and fluorescently labeled phalloidin. α -18 recognizes an epitope of α -catenin that is dependent on the F-actin-mediated pulling force. Scale bars: 10 μm .

Immunoprecipitation experiments showed an interaction between tricellulin and Tuba in MTD-1A cells and in Caco-2 cells (Fig. 4G), indicating that there is an interaction between tricellulin and Tuba in epithelial cells. It has already been reported that Tuba is involved in the regulation of junctional configuration through F-actin organization in Caco-2 cells (Otani et al., 2006). Tricellulin-knockdown Caco-2 cells showed a similar phenotype (Fig. 1F–I), suggesting that the interaction of tricellulin with Tuba is physiologically relevant.

To further demonstrate the role of the tricellulin–Tuba interaction in the behavior of epithelial cells, we generated two strains of tricellulin-knockdown MTD-1A cells stably expressing tricellulin-P48-53A. In these cells, the phenotype of the curved AJC and rosette-like pattern at 48 h after plating was not rescued (Fig. 5A,B). Moreover, at 24 h after plating, the generation of PEC–PEC fibers of F-actin and immunolabeling of the epitope of α -catenin mediated by the F-actin pulling force were much reduced

compared with tricellulin-rescue MTD-1A cells (Fig. 5C). These results strongly suggest that the binding between tricellulin and Tuba is required for the normal configuration of the AJC and F-actin organization during cell–cell junction formation in epithelial cells.

To examine the possibility that tricellulin regulates F-actin organization through a Tuba-independent pathway, Tuba and/or tricellulin were knocked down in Caco-2 cells. If Tuba and tricellulin act independently on F-actin and the junctional configuration, double-knockdown would exhibit an additive phenotype of the individual knockdown effects. When the curved configuration of the AJC and F-actin disorganization were compared between these cells, no additive effect was observed in the tricellulin and Tuba double-knockdown Caco-2 cells compared with tricellulin or Tuba single-knockdown cells (supplementary material Fig. S2B). These results suggest that tricellulin and Tuba act on the cell–cell junction configuration and F-actin organization using the same pathway.

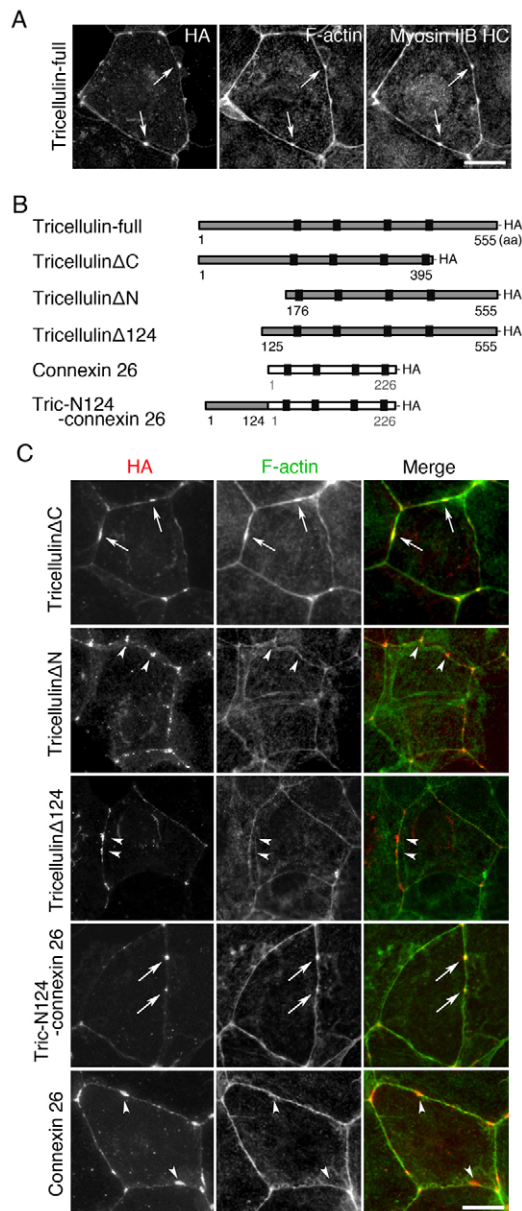


Fig. 3. Role of the N-terminal cytoplasmic domain of tricellulin in the formation of actomyosin clusters. (A) Immunofluorescence staining of EpH4 cells expressing full-length HA-tagged tricellulin with fluorescently labeled phalloidin and an antibody for HA. Exogenous tricellulin sometimes forms aggregates within bicellular cell–cell junctions accompanied by accumulation of F-actin (arrows). (B) Schematic drawings of various deletion and chimeric constructs of tricellulin. Tricellulin-full is a HA-tagged full-length tricellulin. Tricellulin Δ C, tricellulin Δ N and tricellulin Δ 124 lack amino acids 396–555 in the C-terminal cytoplasmic domain, and amino acids 1–175 and amino acids 1–123 in the N-terminal cytoplasmic domain, respectively. Tri-N124-connexin 26 is a chimeric construct of amino acids 1–124 of tricellulin connected with the N-terminus of connexin 26. All constructs were tagged with HA at their C-termini. The black boxes represent transmembrane domains. (C) Double immunofluorescence staining of EpH4 cells expressing the deletion and chimeric constructs of tricellulin shown in B with an anti-HA antibody and fluorescently labeled phalloidin. Aggregates of the tricellulin constructs with and without F-actin clusters are indicated by the arrows and arrowheads, respectively. Scale bars: 10 μ m.

Tuba localizes at cell vertex regions during cell–cell junction formation

Next, to examine the subcellular localization of Tuba, we generated two rabbit polyclonal antibodies against mouse Tuba and a rat polyclonal antibody against mouse tricellulin. Double immunofluorescence staining of MTD-1A cells with one of the anti-mouse-Tuba antibodies and the anti-tricellulin antibody revealed that Tuba and tricellulin were transiently colocalized at PECs at the subconfluent stage during cell–cell junction formation (Fig. 6A, 24 h). This staining pattern of Tuba was also observed with another anti-mouse-Tuba antibody recognizing a different epitope and disappeared when excessive immunogen was added (supplementary material Fig. S3A,B). Furthermore, tricellulin staining at PECs (supplementary material Fig. S3D) and a tricellulin band in western blotting (supplementary material Fig. S3E) were not detected in tricellulin-knockdown cells. These observations demonstrate the specificity of our antibodies against Tuba and tricellulin. Triple labeling of MTD-1A cells with fluorescently labeled phalloidin and anti-Tuba and anti-ZO-1 antibodies showed that F-actin fibers, which were formed at PECs (Fig. 2A,B), came up around the region of Tuba concentration (Fig. 6B). By contrast, we found that Tuba was still localized at PECs in tricellulin-knockdown MTD-1A cells (Fig. 6B), suggesting that Tuba localization is not influenced by tricellulin.

Tricellulin activates Cdc42 through Tuba

Given that the Tuba localization at PECs is independent of tricellulin, a possible role of tricellulin in F-actin formation at PECs might be activation of the Cdc42 GEF activity of Tuba. To examine this idea, conventional pulldown assays with the CRIB domain of WASP in HEK293 cells overexpressing Tuba, its deletion mutants (Fig. 7A) or tricellulin were performed. We found that the GTP-bound active form of endogenous Cdc42 was increased when Tuba was overexpressed compared with the background level of active Cdc42 in HEK293 cells (Fig. 7B,C). Exogenous expression of tricellulin also increased Cdc42 activation and this Cdc42 activation was significantly decreased by shRNA-mediated knockdown of Tuba (Fig. 7B,C). These findings indicate that tricellulin activates Cdc42 through Tuba. It was previously shown that expression of the C-terminal half of Tuba containing the DH, BAR and C-terminal two SH3 domains (Tuba-C) in Caco-2 cells results in greater concentration of E-cadherin at cell–cell contacts than expression of the full-length Tuba (Otani et al., 2006). This observation implies that there is an autoinhibitory mechanism of Tuba in Cdc42 activation, in that the N-terminal half of Tuba interacts with its C-terminal half containing the DH domain and suppresses its GEF activity (Otani et al., 2006). Indeed, the activities of various GEF proteins are modulated by autoinhibition (Bi et al., 2001; Chen et al., 2011; Mitin et al., 2007; Sondermann et al., 2004; Yu et al., 2010). To evaluate this idea, we examined the binding between the N-terminal fragment of Tuba (Tuba-N) and Tuba-C when overexpressed in HEK293 cells. As shown in Fig. 7D, Tuba-N bound to Tuba-C and this interaction was blocked by co-expression of tricellulin, suggesting that Tuba-N competes with tricellulin for Tuba-C binding. Notably, Tuba-C-induced Cdc42 activation in HEK293 cells was inhibited by addition of Tuba-N (Fig. 7E,F) to greater extent than the reduction in endogenous Cdc42 activity caused by sole addition of Tuba-N. Furthermore, the addition of Tuba-N and amino acids 1288–1581 of Tuba, which contained only the fifth and sixth SH3 domains, reduced the Cdc42 activation mediated by tricellulin in a dose-dependent

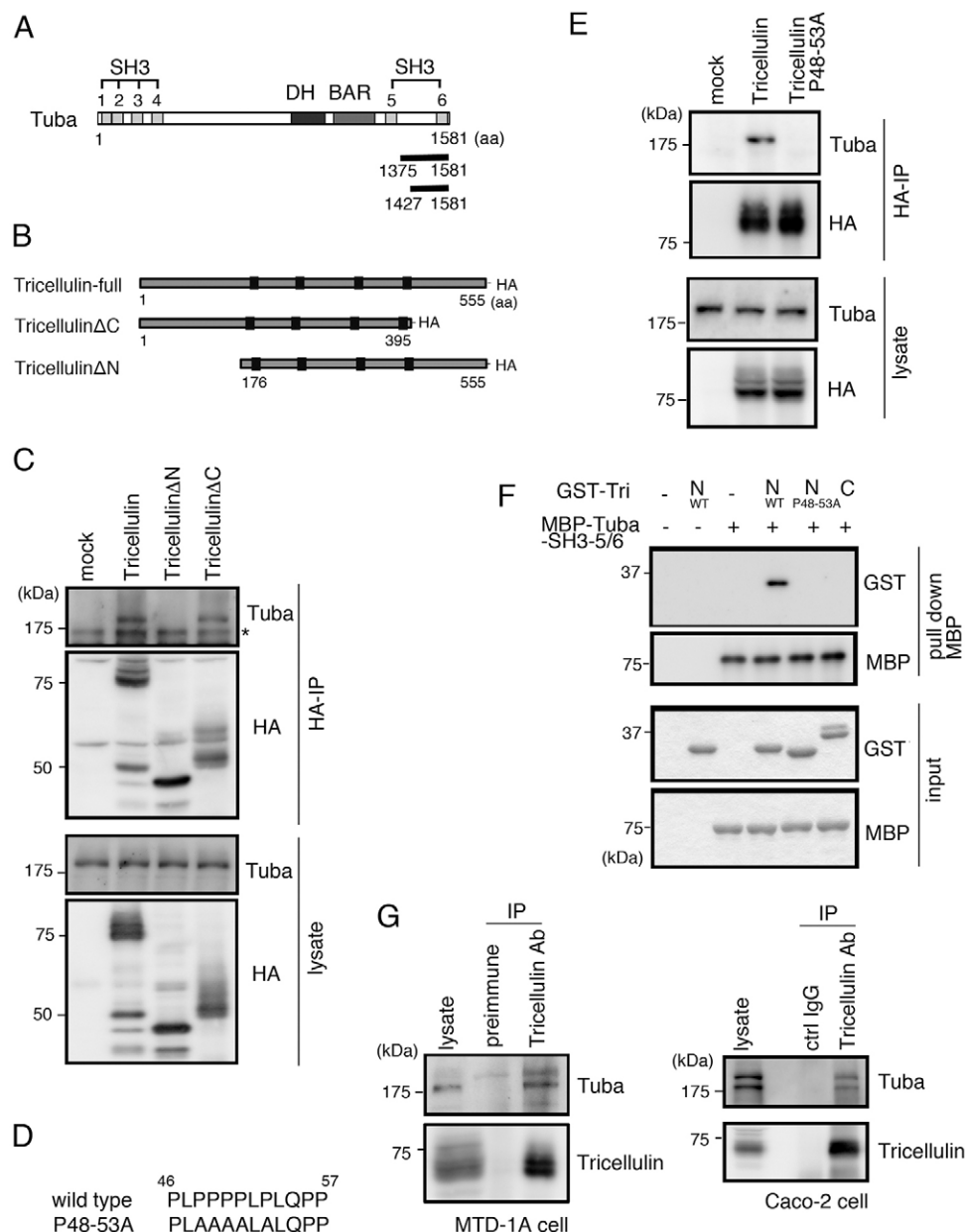


Fig. 4. Tricellulin binds to the Cdc42 GEF Tuba. (A) Schematic representation of Tuba. SH3, Src homology 3 domain; DH, Dbl homology domain; BAR, BAR domain. Tuba has six SH3 domains. Two independent C-terminal fragments of mouse Tuba encoding amino acids 1375–1581 and 1427–1581 (black bars), each of which contained the sixth SH3 domain, were obtained by yeast two-hybrid screening using a bait of amino acids 1–124 of mouse tricellulin. (B) Schematic representation of tricellulin constructs. All constructs were tagged with HA at their C-termini. (C) Interactions of tricellulin with Tuba in immunoprecipitation assays. Lysates of HEK293 cells transfected with a control vector (mock) or expression vectors for HA-tagged tricellulin, tricellulin Δ N and tricellulin Δ C were immunoprecipitated with an anti-HA antibody (HA-IP), followed by immunoblotting with antibodies against Tuba and HA. The asterisk indicates non-specific bands. Immunoblotting of the whole-cell lysates (lysates) is shown in the bottom panels. (D) Amino acid sequences of the proline-rich region at amino acids 46–57 in the N-terminal cytoplasmic domain of mouse tricellulin (wild-type) and of its proline mutant in which five proline residues are replaced with alanine residues (P48-53A). (E) Co-precipitation of Tuba with tricellulin but not with tricellulin P48-53A in immunoprecipitation assays. Lysates of HEK293 cells transfected with a control vector (mock) or expression vectors for HA-tagged tricellulin and tricellulin P48-53A were immunoprecipitated with an anti-HA antibody (HA-IP), followed by immunoblotting with antibodies against Tuba and HA. Immunoblotting of the whole-cell lysates (lysates) is shown in the bottom panels. (F) *In vitro* pull-down assays of GST–tricellulin fusion proteins and a fusion protein of maltose-binding protein (MBP) with the fifth and sixth SH3 domains of Tuba (MBP–Tuba–SH3-5/6). GST-tagged fusion proteins of amino acids 1–150 of tricellulin (N_{WT}), amino acids 1–150 of tricellulin with the P48–53A replacement ($N_{P48-53A}$) and amino acids 396–555 of tricellulin (C) were incubated with MBP–Tuba–SH3-5/6, followed by immunoblotting of the proteins bound to amylose resin with an anti-GST or anti-MBP antibody. The bottom panel indicates Coomassie Brilliant Blue staining of the input MBP or GST fusion proteins. (G) Interaction of endogenous tricellulin and Tuba in MTD-1A cells and Caco-2 cells in immunoprecipitation assays. A whole-cell lysate (lysate) and immunoprecipitates with preimmune rabbit serum and an anti-tricellulin rabbit polyclonal antibody (Tricellulin Ab) for MTD-1A cells or immunoprecipitates with normal rat serum (ctrl IgG) and an anti-tricellulin rat polyclonal antibody (Tricellulin Ab) for Caco-2 cells were immunoblotted with an anti-Tuba antibody and an anti-tricellulin rat monoclonal antibody.

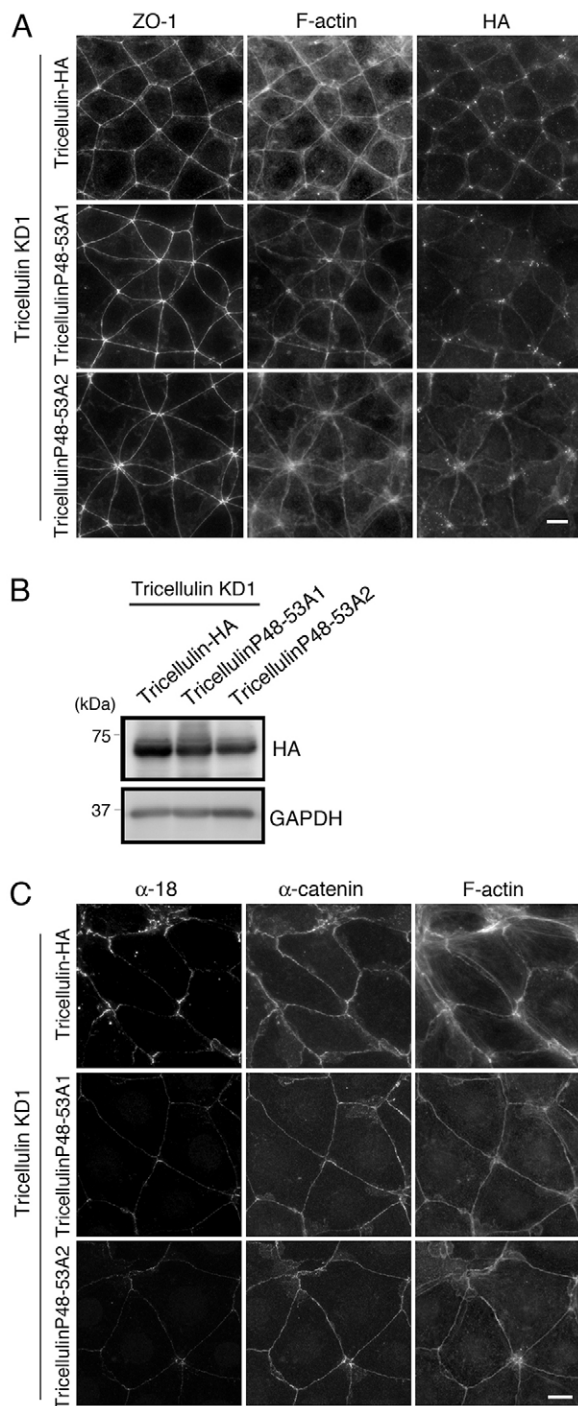


Fig. 5. (A) Immunofluorescence staining of a stable clone of tricellulin-knockdown MTD-1A cells (tricellulin KD1) expressing RNAi-resistant full-length tricellulin with an HA tag (Tricellulin-HA) and two stable clones of tricellulin KD1 cells expressing RNAi-resistant tricellulin P48-53A with an HA tag (Tricellulin P48-53A1 and Tricellulin P48-53A2) using an anti-ZO-1 antibody, fluorescently labeled phalloidin and an anti-HA antibody. Tricellulin P48-53A cannot rescue the curved cell–cell junction phenotype in tricellulin-knockdown MTD-1A cells. (B) Western blotting of the cell lysates shown in A with anti-HA and anti-GAPDH antibodies. (C) Triple immunofluorescence staining of Tricellulin-HA cells, Tricellulin P48-53A1 cells, and Tricellulin P48-53A2 cells at 24 h after plating with the α -18 anti- α -catenin rat monoclonal antibody, an anti- α -catenin rabbit polyclonal antibody and fluorescently labeled phalloidin. α -18 recognizes an epitope of α -catenin that is dependent on the F-actin-mediated pulling force. Scale bars: 10 μ m.

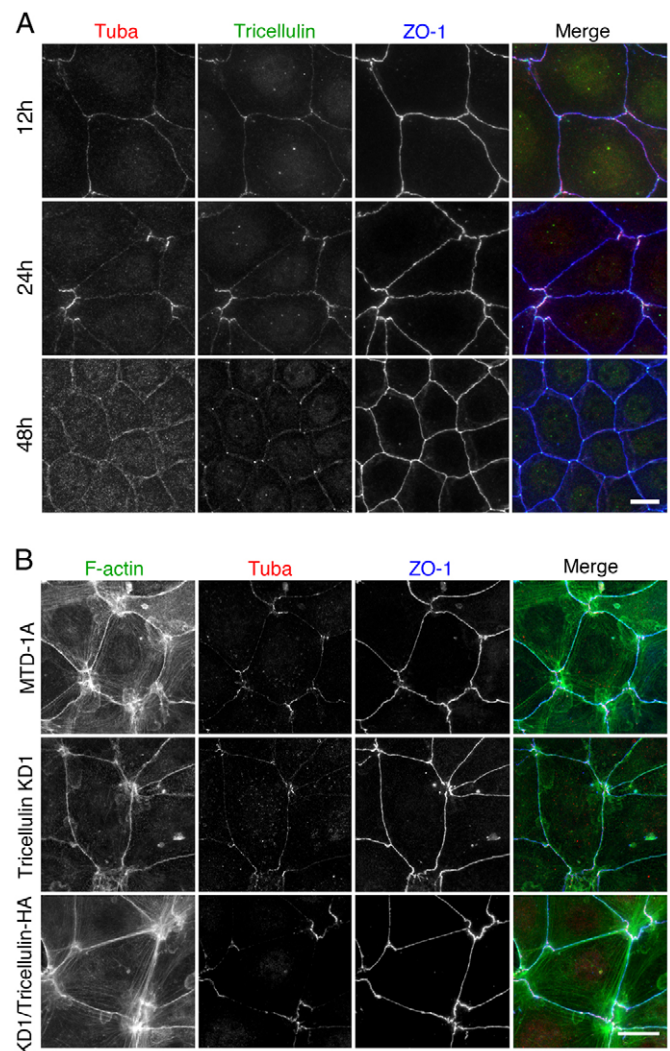


Fig. 6. Localization of Tuba in MTD-1A cells during cell–cell junction formation. (A) Triple immunofluorescence staining of MTD-1A cells with an anti-Tuba rabbit polyclonal antibody, anti-tricellulin rat polyclonal antibody and anti-ZO-1 mouse monoclonal antibody. Cells were fixed at 12, 24 and 48 h after plating. Tuba and tricellulin are transiently colocalized at PECs (24 h). (B) Triple immunofluorescence staining of MTD-1A cells, a stable clone of tricellulin-knockdown MTD-1A cells (Tricellulin KD1) cells and rescue MTD-1A cells (KD1/Tricellulin-HA) cells in a subconfluent condition with an anti-Tuba rabbit polyclonal antibody, anti-ZO-1 monoclonal antibody and fluorescently labeled phalloidin, which visualizes F-actin. F-actin fibers bridging PECs are strongly observed in MTD-1A cells and KD1/Tricellulin-HA cells, but not in tricellulin KD1 cells. Scale bars: 10 μ m.

manner (supplementary material Fig. S4A–E). These findings suggest that the N-terminal half of Tuba interacts with the C-terminal half containing a DH domain and suppresses its GEF activity, and that tricellulin blocks the interaction of Tuba-C with Tuba-N to cancel this autoinhibition (Fig. 7G).

Tricellulin regulates the configuration of cell–cell junctions at tricellular contacts

It is of interest to investigate whether the tricellular contact localization of tricellulin is required for its role in the regulation of the configuration of cell–cell junctions. We have previously shown that the C-terminal cytoplasmic domain of tricellulin is required for its association with angulin family proteins, which

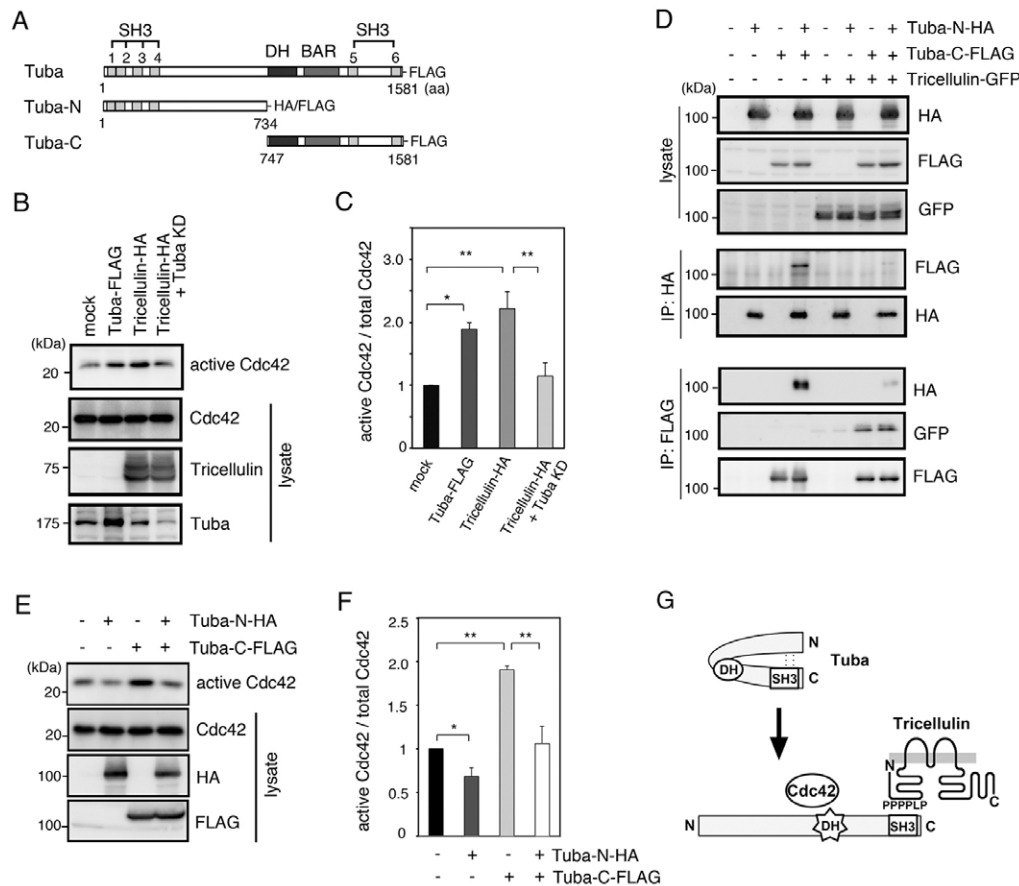


Fig. 7. Tricellulin activates Cdc42 through Tuba by cancelling the autoinhibition of Tuba. (A) Schematic diagrams of the full-length and deletion constructs of Tuba. All constructs were tagged with FLAG or HA at their C-termini. (B) Activation of Cdc42 by tricellulin. HEK293 cells were transfected with a control vector (mock), expression vectors for FLAG-tagged Tuba or HA-tagged tricellulin and the combination of HA-tagged tricellulin and Tuba siRNA (Tuba KD). The active form of Cdc42 (active Cdc42), which bound to a GST–WASP–CRIB fusion protein, was detected by western blotting with an anti-Cdc42 antibody. Tricellulin, Tuba and Cdc42 in the whole-cell lysates are shown in western blotting analyses with antibodies for these proteins (lysate). (C) Quantitative analysis of the active Cdc42 shown in B. The ratio of Cdc42 signals in the GST–WASP–CRIB pulldown samples to those in the total cell lysates was defined as active Cdc42/total Cdc42, relative to the ratio in mock-transfected cells, which was adjusted to 1. Data represent mean \pm s.d. * P < 0.05; ** P < 0.01; n = 4 independent experiments. (D) Interaction between the N-terminal and C-terminal halves of Tuba and its inhibition by tricellulin. HEK293 cells were transfected with expression vectors for HA-tagged Tuba-N, FLAG-tagged Tuba-C and GFP-tagged tricellulin, followed by immunoprecipitation with an anti-HA antibody (IP: HA) and anti-FLAG antibody (IP: FLAG). Whole-cell lysates and the immunoprecipitates were immunoblotted with antibodies against HA, FLAG and GFP. (E) Inhibition of Cdc42 activation by the N-terminal half of Tuba. HEK293 cells were transfected with combinations of the expression vectors for HA-tagged Tuba-N and FLAG-tagged Tuba-C. Whole cell lysates were immunoblotted with antibodies against HA, FLAG and Cdc42. The active form of Cdc42 was detected as shown in B. (F) Quantitative analysis of the active Cdc42 shown in E. The ratio in mock-transfected cells was adjusted to 1. Data represent the mean \pm s.d. * P < 0.05; ** P < 0.01; n = 4 independent experiments. (G) Model for tricellulin-mediated activation of Tuba. The binding of the proline-rich region in the N-terminal cytoplasmic domain of tricellulin (PPPPLP) to the C-terminal SH3 domain of Tuba induces a conformational change of Tuba. This cancels the autoinhibition of Tuba mediated by the interaction between its N-terminal and C-terminal halves, thereby enabling Cdc42 to access to the DH domain of Tuba.

recruit tricellulin to tricellular contacts (Higashi et al., 2013; Masuda et al., 2011), suggesting that tricellulin Δ C would be unable to localize to tricellular contacts. Thus, we introduced tricellulin Δ C into tricellulin-knockdown MTD-1A cells. As expected, the tricellulin Δ C did not concentrate at tricellular contacts and was located throughout the plasma membrane (Fig. 8A,B). The configuration of the cell–cell junctions of these cells still remained curved compared with tricellulin-knockdown MTD-1A cells expressing RNAi-resistant full-length tricellulin, despite the fact that tricellulin Δ C contains the N-terminal cytoplasmic domain, which interacts with Tuba (Fig. 8A,B). These findings indicate that tricellulin regulates the configuration of the AJC at tricellular contacts.

DISCUSSION

Although tricellular contacts have been regarded as intriguing regions for the behavior of polygonal epithelial cells, little is known about their organization and function at the molecular level. In the present study, we found that tricellulin, a tetramembrane spanning protein localizing at tricellular contacts, binds to the Cdc42 GEF Tuba to activate Cdc42 and, hence, controls the organization and tension of actomyosin along the AJC during cell–cell junction formation. Notably, we have shown for the first time that tricellular contacts are involved in the junctional tension and shape determination of epithelial cells at the molecular level. Furthermore, we report here a peculiar mechanism in which a transmembrane protein associated with

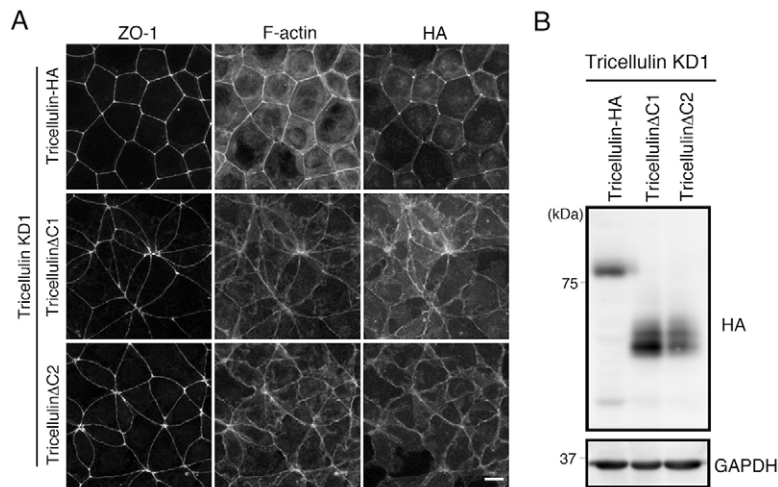


Fig. 8. Tricellulin with the C-terminal cytoplasmic domain deleted cannot rescue the curved cell-cell junction phenotype in tricellulin-knockdown MTD-1A cells. (A) Immunofluorescence staining of a stable clone of tricellulin-knockdown MTD-1A cells (Tricellulin KD1) expressing RNAi-resistant full-length tricellulin with an HA tag (Tricellulin-HA) and two stable clones of tricellulin KD1 expressing tricellulin with the C-terminal cytoplasmic domain deleted tagged with HA (Tricellulin Δ C1 and Tricellulin Δ C2) using an anti-ZO-1 antibody, fluorescently labeled phalloidin and an anti-HA antibody. Scale bar: 10 μ m. (B) Western blotting of lysates from the cells shown in A with anti-HA and anti-GAPDH antibodies.

cell-cell junctions binds to a small G protein GEF to control F-actin organization.

Our yeast two-hybrid screening showed that the sixth SH3 domain at the C-terminus of Tuba is the binding target for the N-terminal cytoplasmic domain of tricellulin. We found that amino acids 1291–1580 of mouse Tuba, which contains the sixth SH3 domain, bound to the N-terminal cytoplasmic domain of tricellulin, which contains a proline-rich region, PLPPPLPLQPP (amino acids 46–57 of mouse tricellulin), and that this binding was impaired when the proline residues were replaced with alanine residues. This finding seems to be a typical case of the interaction between SH3 domains and proline-rich domains (Feller et al., 1994). Our study suggests that the Cdc42 GEF activity of Tuba is autoinhibited by the interaction between the N-terminal half of Tuba and the C-terminal half of Tuba, which contains a DH domain for Cdc42 activation, and that the tricellulin–Tuba interaction cancels this autoinhibition. Indeed, the N-terminal cytoplasmic domain of tricellulin competes with the N-terminal half of Tuba for binding to the C-terminal half of Tuba. The N-terminal half of Tuba also contains a proline-rich region (PPPPRPTPTP, amino acids 609–619), which might bind to the C-terminal SH3 domains of Tuba to mediate autoinhibition, although it remains unclear whether this occurs in an intramolecular or intermolecular manner.

In this study, we analyzed the longest isoform of mouse tricellulin (NM_001038602) and its mutants, but there are several other tricellulin transcripts generated by alternative splicing (Nayak et al., 2013; Riazuddin et al., 2006; Schlüter et al., 2007). In humans, in addition to the longest tricellulin isoform, a shorter isoform, in which the C-terminal ~130 amino acids of the longest form are truncated and replaced with 27 independent amino acids, has been reported. These long and short isoforms are designated tricellulin- α and - β , respectively (Schlüter et al., 2007). To date, the corresponding β isoform in mice is not present in the genome database. We previously examined the behaviors of tricellulin mutant proteins associated with DFN49, for which all the mutations occur within the gene region encoding the C-terminal cytoplasmic domain of tricellulin, using a model system of cultured mouse epithelial cells. We found that none of these mutants, including one with a truncation of ~60 amino acids at the C-terminus, could localize at tricellular contacts (Higashi et al., 2013). In the present study, a mouse tricellulin mutant lacking the C-terminal cytoplasmic domain neither located to tricellular contacts nor rescued the cell configuration phenotype in tricellulin-

knockdown cells, indicating that tricellular contact localization of tricellulin is required for the above tricellulin function mediated by its N-terminal cytoplasmic domain. Taking these observations together, human tricellulin- β is unlikely to be located to tricellular contacts and, hence, be involved in the regulation of F-actin organization and cell-cell junction configuration.

Extensive studies have revealed that myosin II phosphorylation induces contraction of perijunctional actomyosin and affects the behavior of epithelial cell-cell junctions (Cunningham and Turner, 2012; Ivanov et al., 2010). In terms of the signaling pathways required to determine the polygonal shape of epithelial cells, Tuba has been previously reported to regulate the configuration of epithelial cell-cell junctions by mediating Cdc42 activation followed by F-actin assembly along cell-cell junctions through neural Wiskott–Aldrich syndrome protein (N-WASP) (Otani et al., 2006). In addition, the Shroom3–ROCK (Nishimura and Takeichi, 2008), Willin (FRMD6)–aPKC–ROCK (Ishiyuchi and Takeichi, 2011), and Lulu (Epb4115)–p114RhoGEF–Rho–ROCK (Nakajima and Tanoue, 2011; Terry et al., 2011) pathways are involved in the regulation of F-actin at the AJC and influence the junctional configuration. ZO-1 and ZO-2 (also known as TJP1 and TJP2, respectively), which are tight-junction-associated scaffold proteins with structural similarity, have been reported to negatively regulate perijunctional actomyosin tension and affect epithelial cell shape (Fanning et al., 2012). Given that at least Shroom3, Willin and Lulu are located at cell-cell junctions or lateral plasma membranes, they seem to work along the AJC. By contrast, tricellulin is likely to control actomyosin tension through Tuba–Cdc42 at tricellular contacts. When F-actin bundles along the side of polygonal cell-cell junctions stretch by tensile force, they should be connected to tricellular contacts. Thus, tricellulin-triggered F-actin organization through the Tuba–Cdc42 system might play crucial roles in the linkage of F-actin fibers to tricellular contacts as well as the formation of F-actin that bridges between PECs, although the manner of the connection of F-actin with tricellular contacts and its molecular mechanism remain elusive. Given that tTJs extend deeply toward the basal direction along the lateral membranes, it would be of interest to clarify whether F-actin is also organized along tTJs. Downstream of the Cdc42 activation mediated by tricellulin and Tuba, N-WASP, which activates Arp2/3 complex to nucleate actin polymerization (Rohatgi et al., 1999; Machesky et al., 1999), is a plausible effector for

modulating F-actin organization, similar to the previous report that Tuba–Cdc42–N-WASP pathway controls the F-actin assembly along cadherin-based cell–cell junctions and the configuration of epithelial cells (Otani et al., 2006). However, it would be technically difficult to discriminate between the contribution of Tuba–Cdc42–N-WASP to bicellular cell–cell junctions and that to tricellular contacts.

Two mechanisms underlying the generation of the polygonal shape of epithelial cells with straight cell borders have been proposed: a cortical tension generated by actomyosin along cell–cell junctions, and a surface tension of packed cells pushing against each other (Honda et al., 1984; Lecuit and Lenne, 2007). A combination of these two factors, depending on the context, appears to determine the shape of epithelial cells. In our observations, well-developed F-actin fibers bridging between cell corners were transiently observed during cell–cell junction formation. However, after the cell–cell junctions became mature with the increase in cell density, not only the F-actin fibers at the cell boundary but also the tension at tricellular contacts, as evaluated by immunolabeling of the pulling-force-dependent epitope of α -catenin, was not as noticeable. Thus, we speculate that the tricellulin–Tuba–Cdc42 system contributes to the polygonal shape of epithelial cells by generating cortical tension through actomyosin along cell borders when the cells are not tightly packed within the cellular sheet, but its action appears to decrease when the cells become highly packed.

During the intercalation of epithelial cells during dynamic morphogenesis in developmental processes, the lengths of cell–cell junctions change because of the contraction of actomyosin filaments on given sides within polygons of the AJC (Bertet et al., 2004; Blankenship et al., 2006; Fernandez-Gonzalez et al., 2009). In such aspects, tricellular contacts appear not only to withstand tensile forces but also to be dynamically rearranged (Cavey and Lecuit, 2009). It will be of great interest for future studies to investigate how tricellular contacts contribute to such dynamic behaviors of epithelial cells during developmental processes. The potential roles of tricellulin-mediated F-actin organization at tricellular contacts in the epithelial barrier function are also intriguing. RNAi-mediated depletion of tricellulin in mouse EpH4 epithelial cells reduces transepithelial electrical resistance and increased paracellular flux, indicating that tricellulin is required for the full barrier function of epithelial cellular sheets (Ikenouchi et al., 2005). Knockdown of angulin-1/LSR in EpH4 cells also reduces the epithelial barrier function, which is accompanied by a diffuse distribution of tricellulin throughout the plasma membrane (Higashi et al., 2013; Masuda et al., 2011). Taking these studies into account, tricellulin-mediated F-actin regulation at tricellular contacts might also play a crucial role in the maintenance of the epithelial barrier function. Recently, Nayak et al. (Nayak et al., 2013) reported on mice that had a knock-in for tricellulin that mimics one of the mutations of DFNB49 and is predicted to generate a tricellulin mutant protein with a truncation of ~60 amino acids at the C-terminus. The mice grew normally, but suffered from deafness, similar to human patients containing the corresponding tricellulin mutation (Riazuddin et al., 2006). The tricellulin mutant protein was absent from the tricellular contacts of cochlear epithelial cells in the knock-in mice. This is similar to the case for tricellulin Δ C, which cannot locate to tricellular contacts, indicating that the absence of tricellulin from tricellular contacts does not affect the development and growth of mice, but might affect the cochlear barrier, in which a steep gradient of Na⁺ and K⁺ concentrations is

generated between the endolymph and perilymph across the cellular sheet. In addition, it has been reported that tricellular contacts are used as windows wherein protrusions of cells beneath the epithelial cellular sheets penetrate into the lumen to sense the external environment (Kubo et al., 2009; Shum et al., 2008). It is reasonable that the opening and closing of tricellular contacts in such phenomena would be controlled by regulation of actomyosin at tricellular contacts. To better understand the role of actomyosin contraction in the paracellular barrier that prevents the leak of solutes through tricellular contacts, the detailed organization of F-actin at tricellular contacts, including its connection to the plasma membrane, needs to be clarified at the molecular level in future studies.

MATERIALS AND METHODS

Cell culture and transfection

Eph4 cells and Caco-2 cells were kind gifts from Ernst Reichmann (University Children's Hospital Zurich, Zurich, Switzerland) and Takuji Tanoue (RIKEN CDB, Kobe, Japan), respectively. Eph4 cells were cultured in DME supplemented with 10% fetal calf serum. Caco-2 cells were cultured in a 1:1 mixture of DME and Ham's F12 supplemented with 10% fetal calf serum. MTD-1A cells were cloned once by limiting dilution to obtain uniform cells. DNA transfection was performed using the Lipofectamine Plus Reagent (Invitrogen) according to the manufacturer's instructions.

Plasmid construction and siRNAs

The expression vectors for tricellulin with a C-terminal HA or GFP tag, GST-fused tricellulin fragments (Ikenouchi et al., 2005) and its N-terminal or C-terminal deletion mutants with a C-terminal three HAs tag or GFP tag (Masuda et al., 2011) were constructed as described previously. The expression vectors for tricellulin Δ 124 (amino acids 125–555 of mouse tricellulin) and Tric-N124 (amino acids 1–124 of mouse tricellulin) fused with mouse connexin 26 were generated by PCR and subcloned into pCAGGS neodeEcoRI (Niwa et al., 1991) with a C-terminal HA tag. For siRNA-resistant tricellulin expression, targeted sequences of tricellulin were disrupted by site-directed mutagenesis without changing the encoded amino acids. To create the expression vector for the proline mutant of tricellulin (P48-53A), proline residues (amino acids 48, 49, 50, 51 and 53) were changed to alanine residues by site-directed mutagenesis. The expression vectors for Tuba and its deletion mutants were as described previously (Otani et al., 2006). Briefly, they were subcloned into pCA with a C-terminal FLAG or HA tag, pCA with an N-terminal HA tag and pGEX. The expression vectors for GST fusion tricellulin fragments, pGEX-Tri-N and pGEX-Tri-C, were generated by PCR amplification of the mouse tricellulin N-terminus (amino acids 1–150) or C-terminus (amino acids 396–555), which were subcloned into pGEX6P-1 vectors. The siRNA oligonucleotides against human tricellulin (MARVELD2 stealth select HSS 135886–135888) and human Tuba (DNMBP stealth select HSS 118490), as well as negative controls, were purchased from Invitrogen. HSS135886 was the most effective and was used in this study. For mouse tricellulin knockdown, the oligonucleotide sequence 5'-GAACAACTCTCTCACATA-3' (KD1) cloned into pSUPER was used as described previously (Ikenouchi et al., 2005).

Antibodies and reagents

The following primary antibodies were used: mouse monoclonal antibody (mAb) 5G6A3 against human Tuba (Otani et al., 2006) and rat mAb N54 against mouse tricellulin (Ikenouchi et al., 2005) were generated as described previously; and mouse mAb 7.1/13.1 against GFP (Roche), rat mAb 3F10 against HA (Roche), mouse mAb 16B12 against HA (Covance), mouse mAb M2 against FLAG (Sigma, Stratagene), rabbit polyclonal antibody (pAb) against DDDDK (MBL), rabbit pAb against G3PDH (Trevigen), rabbit pAb against human tricellulin (Invitrogen) and mouse mAb against Cdc42 (BD Biosciences), rabbit pAb anti-MBP (New England Biolabs), Ab anti-GST HRP conjugate (Amersham Biosciences), rabbit pAb anti-2P-myosin (Cell Signaling

Technology), rabbit pAb anti-catenin (sigma) were purchased from the indicated sources. Rabbit pAbs against mouse and human tricellulin were raised against GST fusion proteins with the N-terminal domain (amino acids 1–150 of mouse tricellulin and amino acids 1–148 of human tricellulin, respectively). Rat pAb against mouse tricellulin was also raised against GST fused to amino acids 1–150 of mouse tricellulin. Rabbit pAbs against mouse Tuba were raised against GST fusion proteins with fragments encoding amino acids 1376–1518 and 561–710. Mouse anti-ZO-1 mAb T8-754 (Itoh et al., 1991) and rat anti- α -catenin mAb α -18 (Nagafuchi and Tsukita, 1994) were kindly provided by Masahiko Itoh (Dokkyo Medical University, Tochigi, Japan) and Akira Nagafuchi (Nara Medical University, Nara, Japan), respectively. The following secondary antibodies were used: Alexa-Fluor-488-conjugated donkey anti-rat-, anti-mouse- and anti-rabbit-IgG (Invitrogen); Cy3- or Cy5-conjugated goat anti-rat-, anti-mouse- and anti-rabbit-IgG (Jackson Immunoresearch Laboratories); and horseradish-peroxidase-conjugated anti-rat-, anti-mouse- and anti-rabbit-IgG (GE Healthcare). F-actin was visualized using Alexa-Fluor-488-conjugated phalloidin (Invitrogen).

Immunofluorescence staining

Immunostaining of frozen sections and cultured epithelial cells was performed as described previously (Masuda et al., 2011). For experiments using cultured epithelial cells, a thirtieth of the confluent cells from a 10-cm dish were plated on a 35-mm dish containing coverslips. The cells on coverslips were used for immunostaining after culture for 24, 48 or 72 h. Samples were mounted in FluorSave (Calbiochem) and observed with an Olympus IX71 fluorescence photomicroscope, using UPlanS Apo 40 \times /NA 0.9 or UPlan FLN 60 \times /NA 1.25 oil objectives. Image acquisition was performed using a combination of an ORCA-ER cooled CCD camera (Hamamatsu Photonics K.K.) and IPLab image processing software (BD Biosciences). Measurements of the linearity index and circularity were performed using Image J software.

Yeast two-hybrid screening

Yeast two-hybrid screening was performed with a Matchmaker Two-Hybrid System and an 11-day mouse embryo cDNA library (Clontech). Briefly, 7.16×10^6 yeast transformants were plated on synthetic complete medium lacking histidine, leucine, tryptophan and adenine. A total of 120 colonies were picked up and plasmids were obtained from positive clones using a Zymoprep Kit (Zymo Research). The inserts of the plasmids were sequenced.

Immunoprecipitation and pulldown assays

For immunoprecipitation assays, cells were solubilized with RIPA buffer (1% NP-40, 0.05% SDS, 0.2% sodium deoxycholate, 25 mM Hepes-KOH pH 7.5, 150 mM NaCl, 1 mM EDTA and 10% glycerol). Cell lysates were treated with anti-HA and anti-FLAG antibody-bound protein-G–Sepharose 4 Fast Flow (GE Healthcare) and eluted by boiling in Laemmli sample buffer. For Cdc42 activation assays, cell lysates were incubated with the GST-fused WASP CRIB domain (a gift from Yasuyuki Fujita, Hokkaido University, Sapporo, Japan) as described previously (Hogan et al., 2009). For pulldown assays, cells were lysed in ice-cold lysis buffer (50 mM Tris-HCl pH 7.5, 150 mM NaCl, 0.5% NP-40, 1 mM EDTA and 10% glycerol). After centrifugation, the lysates were incubated with glutathione–Sepharose 4B beads (GE Healthcare) coupled to GST fusion proteins for 2 h on ice, and the beads were washed three times with lysis buffer. The complexes were eluted by boiling in 2 \times Laemmli sample buffer supplemented with 10% β -mercaptoethanol. For *in vitro* pulldown assays, MBP-fused proteins were incubated with GST-fused proteins in 200 μ l binding buffer (50 mM Tris-HCl pH 7.5, 5 mM MgCl₂, 100 mM NaCl, 10% Glycerol, 0.5 mg/ml BSA, 1 mM DTT) for 2 h at 4°C. Amylose Resin (New England Biolabs) were added into the reaction mixture and incubated for 2 h at 4°C. After washing with binding buffer, the precipitants were eluted with binding buffer containing 20 mM maltose, and subjected to SDS-PAGE.

Recombinant protein purification

GST, GST–Tricellulin-N and GST–Tricellulin-C were expressed in DH5 α *Escherichia coli* cells and purified by standard procedures. Briefly, protein expression was induced by addition of 0.1 mM IPTG to bacterial

cultures, and proteins were expressed at 37°C for 3 h. The cells were collected by centrifugation and lysed by sonication in phosphate-buffered saline (PBS). Triton X-100 (final concentration, 1%) was added to the sonicated lysates, followed by incubation for 30 min at 4°C and clarification by centrifugation. Subsequently, the supernatants were incubated with glutathione–Sepharose beads (GE Healthcare) for 1 h, and the beads were washed three times with PBS, twice with wash buffer (PBS containing 1 M NaCl) and twice with PBS. The bound proteins were eluted with elution buffer (50 mM Tris-HCl pH 8.0, 20 mM glutathione), and the eluted proteins were dialyzed against 20 mM Tris-HCl (pH 7.5) using a Slide-A-Lyzer Dialysis cassette (10K MWCO; Thermo Scientific). The purified proteins were either used immediately or supplemented with 10% glycerol and stored at –80°C until use.

Western blotting

For western blotting, proteins were separated by SDS-PAGE and transferred onto Immobilon-P PVDF membranes (Millipore). Signals were detected using an ECL chemiluminescence system (GE Healthcare) and an LAS-3000 mini imaging system (Fujifilm).

Statistical analysis

Means and s.d. were calculated. The respective *n* values are shown in the figure legends. The indicated *P* values were obtained with a one-tailed Student's *t*-test.

Quantification of cell shape

The junction length, which was indicated by the length of ZO-1 staining between two vertices, and the distance between these vertices were measured. The linearity index was defined by the ratio of the junction length to the distance between the vertices. Three independent experiments were performed, in each of which >30 junctions were randomly selected and measured. To quantify the number of rosette-like structures in cell–cell junctions, the number of regions where more than five cell vertices delineated by ZO-1 staining were crowded together within a circle of 5- μ m diameter in 32400 μ m² was counted. Three independent measurements were performed. The circularity index was defined by the ratio of $4\pi \times$ apical surface area to the square of the perimeter, which reflects a compactness measure of each cell shape. Three independent experiments were performed, in each of which >30 cells were randomly selected and measured, followed by Student's *t*-test analysis.

Acknowledgements

We thank Takuji Tanoue, Yasuyuki Fujita, Ernst Reichmann and Akira Nagafuchi for cells and reagents; Tomoko Kato for technical assistance and Masatoshi Takeichi, Akira Nagafuchi, Shigenobu Yonemura, Hisao Honda and all the members of the Furuse laboratory for their helpful discussions.

Competing interests

The authors declare no competing interests.

Author contributions

Y.O. and M.F. designed and wrote the manuscript. Y.O. and T.O. performed the experiments. J.I. provided the materials.

Funding

This work was supported in part by the Funding Program for Next Generation World Leading Researchers (NEXT Program) from the Japan Society for the Promotion of Science (JSPS) [grant number LS084 to M.F.]; a Grant-in-Aid for Scientific Research (B) from JSPS [grant number 26291043 to M.F.]; and a Grant-in-Aid for Scientific Research (C) from JSPS [grant number 23570229 to Y.O.].

Supplementary material

Supplementary material available online at <http://jcs.biologists.org/lookup/suppl/doi:10.1242/jcs.150607/-DC1>

References

- Bertet, C., Sulak, L. and Lecuit, T. (2004). Myosin-dependent junction remodelling controls planar cell intercalation and axis elongation. *Nature* **429**, 667–671.
- Bi, F., Debreceni, B., Zhu, K., Salani, B., Eva, A. and Zheng, Y. (2001). Autoinhibition mechanism of proto-Dbl. *Mol. Cell. Biol.* **21**, 1463–1474.

- Blankenship, J. T., Backovic, S. T., Sanny, J. S., Weitz, O. and Zallen, J. A. (2006). Multicellular rosette formation links planar cell polarity to tissue morphogenesis. *Dev. Cell* **11**, 459–470.
- Cavey, M. and Lecuit, T. (2009). Molecular bases of cell-cell junctions stability and dynamics. *Cold Spring Harb. Perspect. Biol.* **1**, a002998.
- Chen, Z., Guo, L., Sprang, S. R. and Sternweis, P. C. (2011). Modulation of a GEF switch: autoinhibition of the intrinsic guanine nucleotide exchange activity of p115-RhoGEF. *Protein Sci.* **20**, 107–117.
- Cunningham, K. E. and Turner, J. R. (2012). Myosin light chain kinase: pulling the strings of epithelial tight junction function. *Ann. N. Y. Acad. Sci.* **1258**, 34–42.
- Fanning, A. S., Van Itallie, C. M. and Anderson, J. M. (2012). Zonula occludens-1 and -2 regulate apical cell structure and the zonula adherens cytoskeleton in polarized epithelia. *Mol. Biol. Cell* **23**, 577–590.
- Farquhar, M. G. and Palade, G. E. (1963). Junctional complexes in various epithelia. *J. Cell Biol.* **17**, 375–412.
- Feller, S. M., Ren, R., Hanafusa, H. and Baltimore, D. (1994). SH2 and SH3 domains as molecular adhesives: the interactions of Crk and Abl. *Trends Biochem. Sci.* **19**, 453–458.
- Fernandez-Gonzalez, R., Simoes, S. M., Röper, J. C., Eaton, S. and Zallen, J. A. (2009). Myosin II dynamics are regulated by tension in intercalating cells. *Dev. Cell* **17**, 736–743.
- Gumbiner, B. M. (2005). Regulation of cadherin-mediated adhesion in morphogenesis. *Nat. Rev. Mol. Cell Biol.* **6**, 622–634.
- Higashi, T., Tokuda, S., Kitajiri, S., Masuda, S., Nakamura, H., Oda, Y. and Furuse, M. (2013). Analysis of the 'angulin' proteins LSR, ILDR1 and ILDR2 – tricellulin recruitment, epithelial barrier function and implication in deafness pathogenesis. *J. Cell Sci.* **126**, 966–977.
- Hogan, C., Dupré-Crochet, S., Norman, M., Kajita, M., Zimmermann, C., Pelling, A. E., Piddini, E., Baena-López, L. A., Vincent, J. P., Itoh, Y. et al. (2009). Characterization of the interface between normal and transformed epithelial cells. *Nat. Cell Biol.* **11**, 460–467.
- Honda, H. (1983). Geometrical models for cells in tissues. *Int. Rev. Cytol.* **81**, 191–248.
- Honda, H. and Eguchi, G. (1980). How much does the cell boundary contract in a monolayered cell sheet? *J. Theor. Biol.* **84**, 575–588.
- Honda, H., Ogita, Y., Higuchi, S. and Kani, K. (1982). Cell movements in a living mammalian tissue: long-term observation of individual cells in wounded corneal endothelia of cats. *J. Morphol.* **174**, 25–39.
- Honda, H., Dan-Sohkawa, M. and Watanabe, K. (1984). Geometrical analysis of cells becoming organized into a tensile sheet, the blastular wall, in the starfish. *Differentiation* **25**, 16–22.
- Ikenouchi, J., Furuse, M., Furuse, K., Sasaki, H., Tsukita, S. and Tsukita, S. (2005). Tricellulin constitutes a novel barrier at tricellular contacts of epithelial cells. *J. Cell Biol.* **171**, 939–945.
- Ikenouchi, J., Sasaki, H., Tsukita, S., Furuse, M. and Tsukita, S. (2008). Loss of occludin affects tricellular localization of tricellulin. *Mol. Biol. Cell* **19**, 4687–4693.
- Ishiuchi, T. and Takeichi, M. (2011). Willin and Par3 cooperatively regulate epithelial apical constriction through aPKC-mediated ROCK phosphorylation. *Nat. Cell Biol.* **13**, 860–866.
- Itoh, M., Yonemura, S., Nagafuchi, A., Tsukita, S. and Tsukita, S. (1991). A 220-kD undercoat-constitutive protein: its specific localization at cadherin-based cell-cell adhesion sites. *J. Cell Biol.* **115**, 1449–1462.
- Ivanov, A. I., Parkos, C. A. and Nusrat, A. (2010). Cytoskeletal regulation of epithelial barrier function during inflammation. *Am. J. Pathol.* **177**, 512–524.
- Jaffe, A. B. and Hall, A. (2005). Rho GTPases: biochemistry and biology. *Annu. Rev. Cell Dev. Biol.* **21**, 247–269.
- Kubo, A., Nagao, K., Yokouchi, M., Sasaki, H. and Amagai, M. (2009). External antigen uptake by Langerhans cells with reorganization of epidermal tight junction barriers. *J. Exp. Med.* **206**, 2937–2946.
- Lecuit, T. and Lenne, P. F. (2007). Cell surface mechanics and the control of cell shape, tissue patterns and morphogenesis. *Nat. Rev. Mol. Cell Biol.* **8**, 633–644.
- Lecuit, T., Lenne, P. F. and Munro, E. (2011). Force generation, transmission, and integration during cell and tissue morphogenesis. *Annu. Rev. Cell Dev. Biol.* **27**, 157–184.
- Machesky, L. M., Mullins, R. D., Higgs, H. N., Kaiser, D. A., Blanchoin, L., May, R. C., Hall, M. E. and Pollard, T. D. (1999). Scar, a WASp-related protein, activates nucleation of actin filaments by the Arp2/3 complex. *Proc. Natl. Acad. Sci. USA* **96**, 3739–3744.
- Masuda, S., Oda, Y., Sasaki, H., Ikenouchi, J., Higashi, T., Akashi, M., Nishi, E. and Furuse, M. (2011). LSR defines cell corners for tricellular tight junction formation in epithelial cells. *J. Cell Sci.* **124**, 548–555.
- Mitn, N., Betts, L., Yohe, M. E., Der, C. J., Sondek, J. and Rossman, K. L. (2007). Release of autoinhibition of ASEF by APC leads to CDC42 activation and tumor suppression. *Nat. Struct. Mol. Biol.* **14**, 814–823.
- Nagafuchi, A. and Tsukita, S. (1994). The loss of the expression of alpha catenin, the 102 kD cadherin associated protein, in central nervous tissues during development. *Dev. Growth Differ.* **36**, 59–71.
- Nakajima, H. and Tanoue, T. (2011). Lulu2 regulates the circumferential actomyosin tensile system in epithelial cells through p114RhoGEF. *J. Cell Biol.* **195**, 245–261.
- Nayak, G., Lee, S. I., Yousaf, R., Edelmann, S. E., Trincot, C., Van Itallie, C. M., Sinha, G. P., Rafeeq, M., Jones, S. M., Belyantseva, I. A. et al. (2013). Tricellulin deficiency affects tight junction architecture and cochlear hair cells. *J. Clin. Invest.* **123**, 4036–4049.
- Nishimura, T. and Takeichi, M. (2008). Shroom3-mediated recruitment of Rho kinases to the apical cell junctions regulates epithelial and neuroepithelial planar remodeling. *Development* **135**, 1493–1502.
- Niwa, H., Yamamura, K. and Miyazaki, J. (1991). Efficient selection for high-expression transfectants with a novel eukaryotic vector. *Gene* **108**, 193–199.
- Otani, T., Ichii, T., Aono, S. and Takeichi, M. (2006). Cdc42 GEF Tuba regulates the junctional configuration of simple epithelial cells. *J. Cell Biol.* **175**, 135–146.
- Raleigh, D. R., Marchiando, A. M., Zhang, Y., Shen, L., Sasaki, H., Wang, Y., Long, M. and Turner, J. R. (2010). Tight junction-associated MARVEL proteins marvel3, tricellulin, and occludin have distinct but overlapping functions. *Mol. Biol. Cell* **21**, 1200–1213.
- Riazuddin, S., Ahmed, Z. M., Fanning, A. S., Lagziel, A., Kitajiri, S., Ramzan, K., Khan, S. N., Chattaraj, P., Friedman, P. L., Anderson, J. M. et al. (2006). Tricellulin is a tight-junction protein necessary for hearing. *Am. J. Hum. Genet.* **79**, 1040–1051.
- Rohatgi, R., Ma, L., Miki, H., Lopez, M., Kirchhausen, T., Takenawa, T. and Kirschner, M. W. (1999). The interaction between N-WASP and the Arp2/3 complex links Cdc42-dependent signals to actin assembly. *Cell* **97**, 221–231.
- Salazar, M. A., Kwiatkowski, A. V., Pellegrini, L., Cestra, G., Butler, M. H., Rossman, K. L., Serna, D. M., Sondek, J., Gertler, F. B. and De Camilli, P. (2003). Tuba, a novel protein containing bin/amphiphysin/Rvs and Dbl homology domains, links dynamin to regulation of the actin cytoskeleton. *J. Biol. Chem.* **278**, 49031–49043.
- Schlüter, H., Moll, I., Wolburg, H. and Franke, W. W. (2007). The different structures containing tight junction proteins in epidermal and other stratified epithelial cells, including squamous cell metaplasia. *Eur. J. Cell Biol.* **86**, 645–655.
- Shum, W. W., Da Silva, N., McKee, M., Smith, P. J., Brown, D. and Breton, S. (2008). Transepithelial projections from basal cells are luminal sensors in pseudostratified epithelia. *Cell* **135**, 1108–1117.
- Smutny, M., Cox, H. L., Leerberg, J. M., Kovacs, E. M., Conti, M. A., Ferguson, C., Hamilton, N. A., Parton, R. G., Adelstein, R. S. and Yap, A. S. (2010). Myosin II isoforms identify distinct functional modules that support integrity of the epithelial zonula adherens. *Nat. Cell Biol.* **12**, 696–702.
- Sondermann, H., Soisson, S. M., Boykevich, S., Yang, S. S., Bar-Sagi, D. and Kuriyan, J. (2004). Structural analysis of autoinhibition in the Ras activator Son of sevenless. *Cell* **119**, 393–405.
- Steed, E., Rodrigues, N. T., Balda, M. S. and Matter, K. (2009). Identification of MarvelD3 as a tight junction-associated transmembrane protein of the occludin family. *BMC Cell Biol.* **10**, 95.
- Terry, S. J., Zihni, C., Elbediwy, A., Vitiello, E., Leefa Chong San, I. V., Balda, M. S. and Matter, K. (2011). Spatially restricted activation of RhoA signalling at epithelial junctions by p114RhoGEF drives junction formation and morphogenesis. *Nat. Cell Biol.* **13**, 159–166.
- Vichas, A. and Zallen, J. A. (2011). Translating cell polarity into tissue elongation. *Semin. Cell Dev. Biol.* **22**, 858–864.
- Watanabe, T., Hosoya, H. and Yonemura, S. (2007). Regulation of myosin II dynamics by phosphorylation and dephosphorylation of its light chain in epithelial cells. *Mol. Biol. Cell* **18**, 605–616.
- Yamada, S. and Nelson, W. J. (2007). Localized zones of Rho and Rac activities drive initiation and expansion of epithelial cell-cell adhesion. *J. Cell Biol.* **178**, 517–527.
- Yonemura, S. (2011). Cadherin-actin interactions at adherens junctions. *Curr. Opin. Cell Biol.* **23**, 515–522.
- Yonemura, S., Wada, Y., Watanabe, T., Nagafuchi, A. and Shibata, M. (2010). alpha-Catenin as a tension transducer that induces adherens junction development. *Nat. Cell Biol.* **12**, 533–542.
- Yu, B., Martins, I. R., Li, P., Amarasinghe, G. K., Umetani, J., Fernandez-Zapico, M. E., Billadeau, D. D., Machius, M., Tomchick, D. R. and Rosen, M. K. (2010). Structural and energetic mechanisms of cooperative autoinhibition and activation of Vav1. *Cell* **140**, 246–256.

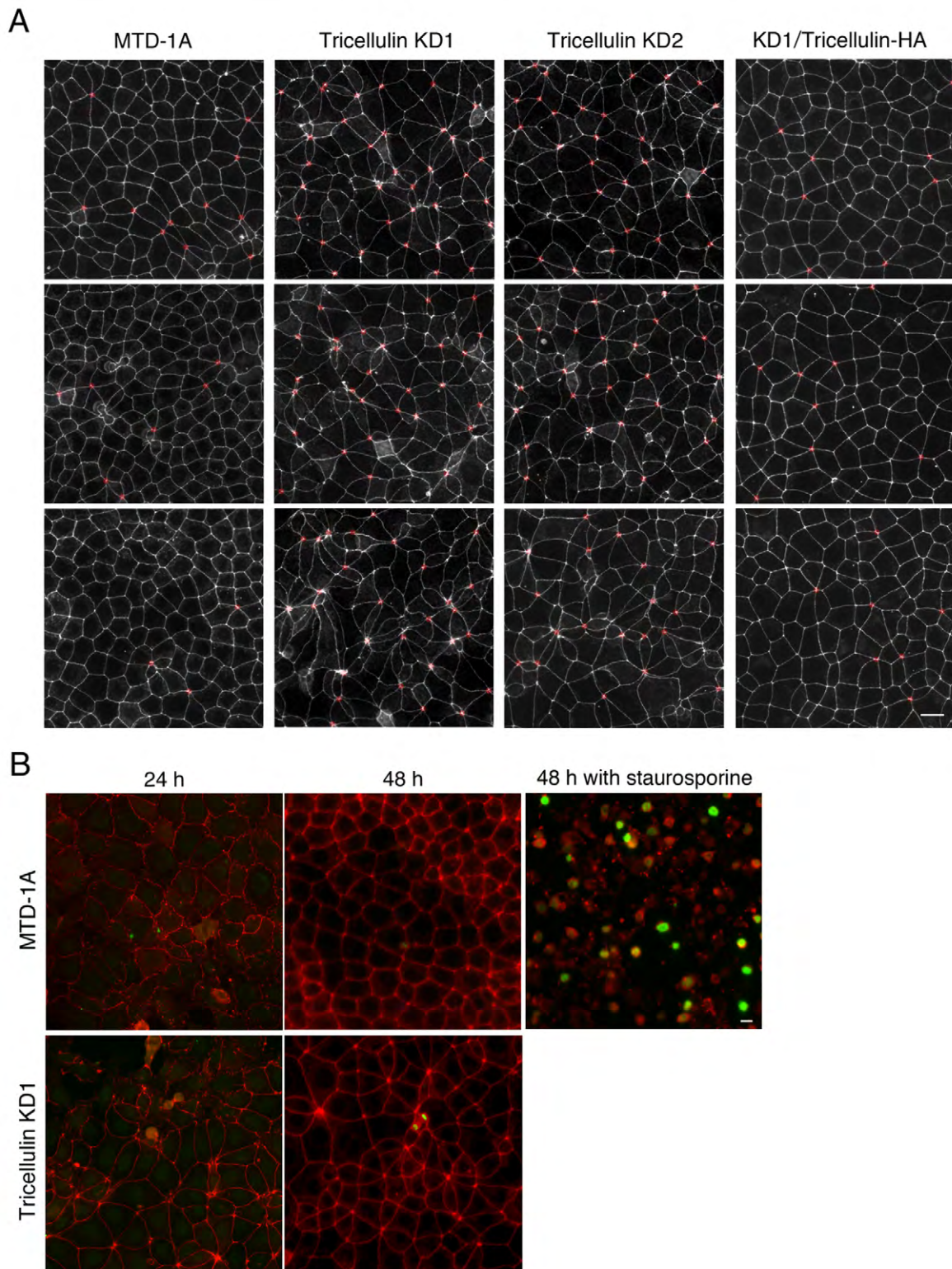


Fig. S1. (A) Original images for quantification of the number of rosette-like structures in MTD-1A cells and two clones of tricellulin knockdown cells (Tricellulin KD1 and Tricellulin KD2) presented in Figure 1D. The numbers of regions where more than five cell vertices were crowded together within a circle of 5-mm diameter (red circles) in immunofluorescence staining images with an anti-ZO-1 antibody were counted. Three independent measurements were performed for each cell type. Bar, 20 mm. (B) TUNEL assays of tricellulin knockdown MTD-1A cells during rosette-like structure formation. MTD-1A cells and Tricellulin KD1 cells at 24 and 48 h after plating were processed for TUNEL assays using a Click-it TUNEL Imaging Assay (Molecular Probes). As a positive control for apoptosis, MTD-1A cells at 24 h after plating were treated with 5 mM staurosporine for 3 h, cultured with normal medium for a further 21 h, and then processed for TUNEL assays. Each panel shows the merged image of apoptotic nuclei (green) and immunostaining for ZO-1 (red). At each time point for Tricellulin KD1 cells, apoptotic nuclei are hardly detected, suggesting that the rosette-like structures of Tricellulin KD1 cells observed at 48 h after plating are not caused by cell extrusion from the cellular sheet via apoptosis. Bar, 10 mm.

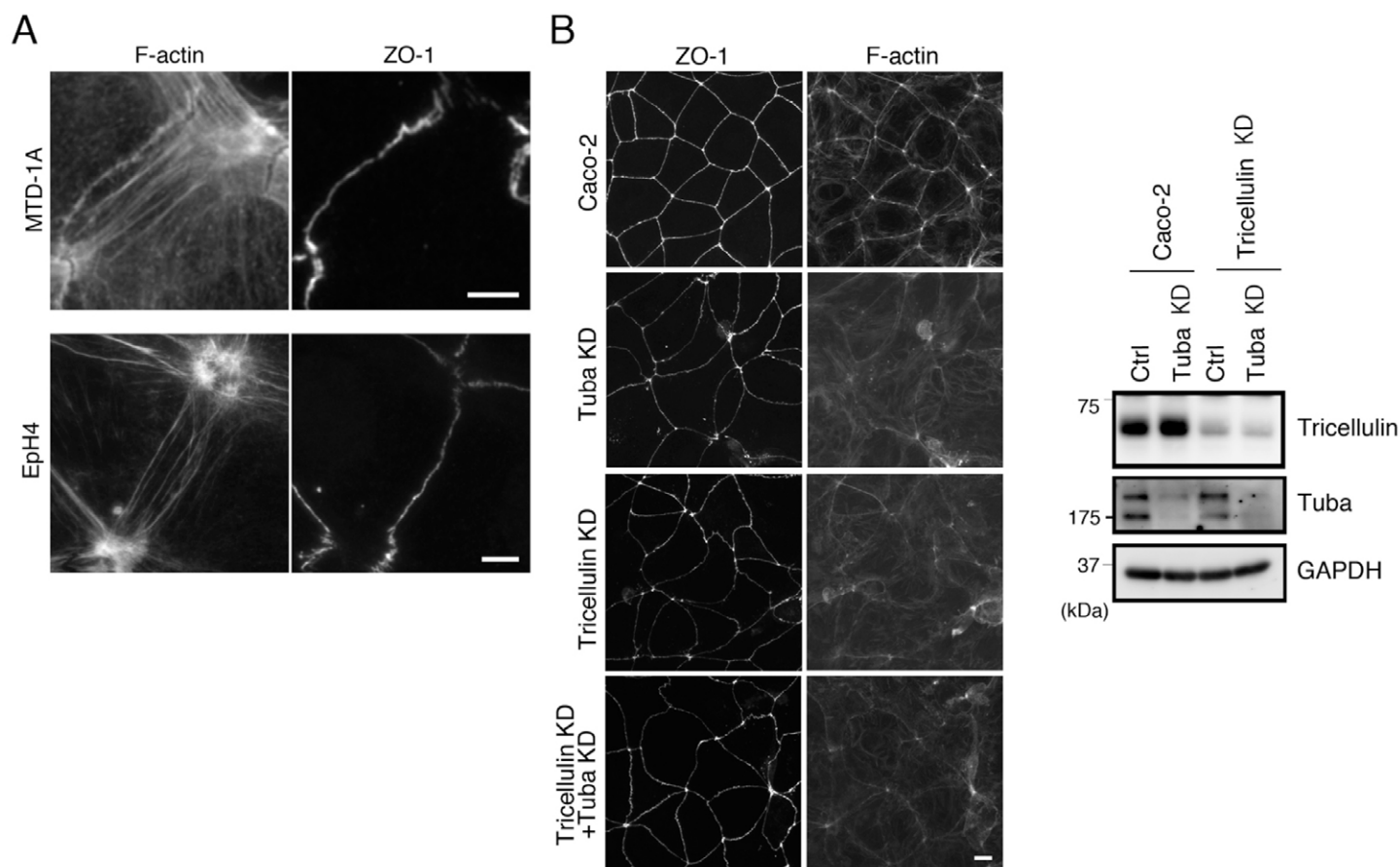


Fig. S2. (A) High-magnification images of PEC-PEC F-actin fibers. PEC-PEC fibers of F-actin in MTD-1A cells and Eph4 cells were visualized by fluorescent phalloidin staining. The cells were counterstained with an anti-ZO-1 antibody to delineate cell-cell junctions. The experimental conditions are the same as those for Figure 2A, B. Bars, 5 mm. (B) Immunofluorescence staining of Caco-2 cells, Tuba siRNA-treated Caco-2 cells (Tuba KD), tricellulin siRNA-treated Caco-2 cells (Tricellulin KD), and Caco-2 cells treated with both tricellulin siRNA and Tuba siRNA (Tricellulin KD+Tuba KD) at 48 h after plating using an anti-ZO-1 antibody with fluorescently labeled phalloidin. Bar, 10 mm. The immunoblots indicate the expressions of tricellulin and Tuba in Caco-2 cells, Tuba siRNA-treated Caco-2 cells, tricellulin siRNA-treated Caco-2 cells, and Caco-2 cells treated with both tricellulin siRNA and Tuba siRNA from the left.

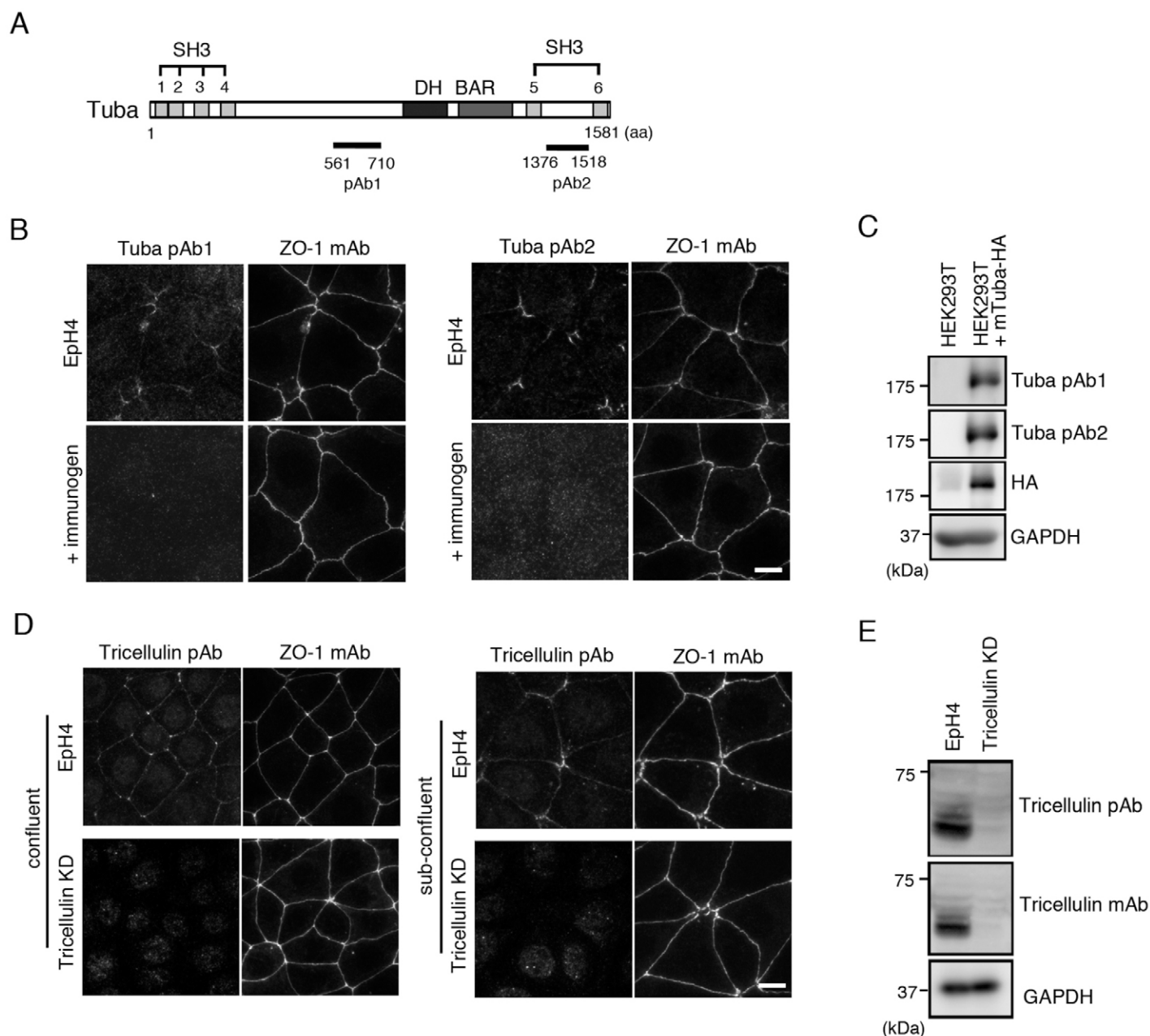


Fig. S3. Characterization of rabbit anti-mouse Tuba polyclonal antibodies and a rat anti-tricellulin polyclonal antibody. (A) Schematic representation of mouse Tuba, which contains six SH3 domains, one DH domain and one BAR domain. Rabbit anti-Tuba polyclonal antibodies 1 (pAb1) and 2 (pAb2) were raised against GST fusion proteins with aa 561–710 and aa 1376–1518 of mouse Tuba, respectively. (B) Immunofluorescence staining of EpH4 cells in a subconfluent condition with anti-Tuba antibodies pAb1 and pAb2 in the absence and presence of their corresponding immunogens. Both antibodies show identical staining patterns at cell corner regions, and this staining disappears after addition of their immunogens, indicating the specificity of these antibodies in immunofluorescence staining. The cells were counterstained with a mouse anti-ZO-1 monoclonal antibody to delineate cell–cell contacts. Bar, 10 μ m. (C) Western blotting of HEK293 cells transfected with control vector or an expression vector for mouse Tuba-HA using two anti-Tuba antibodies (pAb1 and pAb2), an anti-HA antibody and an anti-GAPDH antibody. (D) Double immunofluorescence staining of EpH4 cells and tricellulin knockdown EpH4 cells (Tricellulin KD) in confluent and subconfluent conditions with a rat anti-tricellulin polyclonal antibody (Tricellulin pAb) and a mouse anti-ZO-1 monoclonal antibody. The characteristic staining pattern of tricellulin at cell corner regions of subconfluent EpH4 cells is not detected in Tricellulin KD cells, indicating that this staining is tricellulin-specific. Bars, 10 μ m. (E) Western blotting of EpH4 and Tricellulin KD cells with antibodies for tricellulin and GAPDH.

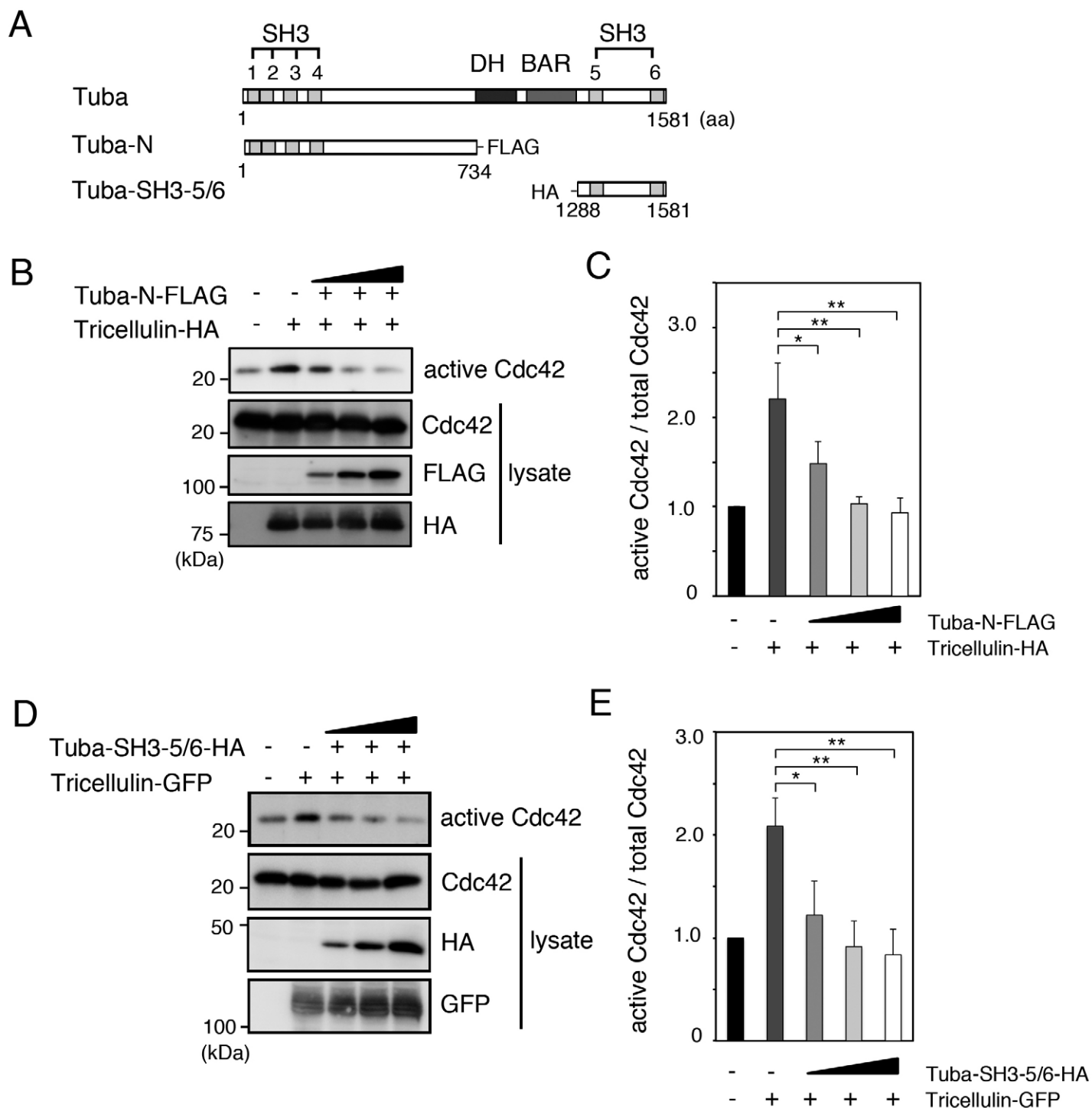


Fig. S4. Inhibition of tricellulin-mediated Cdc42 activation by the addition of Tuba fragments. (A) Schematic diagrams of full-length Tuba and its deletion constructs. Tuba-SH3-5/6 contains only the fifth and sixth SH3 domains tagged with HA. (B) Inhibition of tricellulin-induced Cdc42 activation by expression of the N-terminal half of Tuba. HEK293 cells were transfected with expression vectors for HA-tagged tricellulin and FLAG-tagged Tuba-N, which were added in a dose-dependent manner. The active form of Cdc42 was detected as shown in Fig. 7B. Whole cell lysates (lysate) were immunoblotted with antibodies for HA, FLAG and Cdc42. (C) Quantitative analysis of active Cdc42 in (B) calculated according to the method in Fig. 7C. (D) Inhibition of tricellulin-induced Cdc42 activation by expression of the C-terminal fragment of Tuba containing the C-terminal two SH3 domains. HEK293 cells were transfected with expression vectors for GFP-tagged tricellulin and HA-tagged Tuba-SH3-5/6, which were added in a dose-dependent manner. The active form of Cdc42 was detected as shown in Fig. 7B. Whole cell lysates (lysate) were immunoblotted with antibodies for HA, GFP and Cdc42. (E) Quantitative analysis of active Cdc42 in (D) calculated according to the method in Fig. 7C.